© 2018. Published by The Company of Biologists Ltd | Journal of Cell Science (2018) 131, jcs209361. doi:10.1242/jcs.209361

RESEARCH ARTICLE

EFA6 proteins regulate lumen formation through α-actinin 1

Julie Milanini[1], Racha Fayad[1], Mariagrazia Partisani[1], Patrick Lecine[2,*], Jean-Paul Borg[2], Michel Franco[1] and Frédéric Luton[1,‡]

ABSTRACT

A key step of epithelial morphogenesis is the creation of the lumen. Luminogenesis by hollowing proceeds through the fusion of apical vesicles at cell–cell contacts. The small nascent lumens grow through extension, coalescence and enlargement, coordinated with cell division, to give rise to a single central lumen. Here, by using MDCK cells grown in 3D-culture, we show that EFA6A (also known as PSD) participates in luminogenesis. EFA6A recruits α-actinin 1 (ACTN1) through direct binding. In polarized cells, ACTN1 was found to be enriched at the tight junction where it acts as a primary effector of EFA6A for normal luminogenesis. Both proteins are essential for the lumen extension and enlargement, where they mediate their effect by regulating the cortical acto-myosin contractility. Finally, ACTN1 was also found to act as an effector for the isoform EFA6B (also known as PSD4) in the human mammary tumoral MCF7 cell line. EFA6B restored the glandular morphology of this tumoral cell line in an ACTN1-dependent manner. Thus, we identified new regulators of cyst luminogenesis essential for the proper maturation of a newly-formed lumen into a single central lumen.

KEY WORDS: Epithelium, Lumen, EFA6, ACTN1, Contractility

INTRODUCTION

During organogenesis, the coordinated establishment of the apico-basal polarity with the *de novo* formation of an apical luminal space is fundamental to the emergence of the different types of epithelia. In adult organisms, the aptitude of the internal organs, which are lined with epithelial tissues, to ensure specific functions relies on the preservation of these characteristics. The failure in doing so is associated with a large variety of diseases (Blasky et al., 2015; Datta et al., 2011; Sigurbjörnsdóttir et al., 2014). In particular, these features are often compromised in carcinomas and tumors are formed of non-polarized cell aggregates incapable of collectively organizing a lumen (Martin-Belmonte and Perez-Moreno, 2011; Tanos and Rodriguez-Boulan, 2008; Wang et al., 2012). However, compelling tumoral cells to maintain their normal epithelial phenotype can help them override the power of oncogenes (DuFort et al., 2011; Weaver et al., 1997). Thus, it is important to decipher the molecular programs that instruct epithelial cells to collectively organize around lumens in order to maintain their physiological homeostasis.

For most epithelial tissues, the *de novo* formation of a lumen is generated by hollowing. In this process, apical vesicles are delivered to a focal point of the cell–cell contact named the apical membrane initiation site (AMIS) to give rise to the apical plasma membrane and a facing hollow cavity. The nascent lumen appears first as a closed elongated space named the pre-apical patch (PAP), which is limited by tight junctions. The PAP will then open and expand through a combination of events: the delivery of vesicular membranes, the repulsion of the apposed membrane by highly charged molecules, the increase of hydrostatic pressure, the coalescence of mini-lumens and, eventually, expansion through cell division. This process is closely synchronized with a profound rearrangement of the actin cytoskeleton into discrete structures essential for the attachment of structural and signaling apical proteins. These proteins will then yield a scaffold to shape the lumen and form an acto-myosin ring in support of the circumferential apical junctional complexes (AJCs), which are made of adherens junctions (AJs) and the apical tight junctions (TJs) that outline the luminal space (Datta et al., 2011; Sigurbjörnsdóttir et al., 2014). The organization and functions of the acto-myosin ring attached to the AJ have been extensively studied (Arnold et al., 2017; Braga, 2016; Grikscheit and Grosse, 2016; Lecuit and Yap, 2015); however, far less is known about the actin cytoskeleton associated to the TJ. Nevertheless, it is likely that both structures are somehow intermingled within the so-called apical perijunctional acto-myosin ring (PAMR) (Ebrahim et al., 2013; Sluysmans et al., 2017). The PAMR is described as a sarcomeric-like belt made of F-actin bundles containing myosin-II, which confers contractile properties, and bundling proteins, such as the non-muscle α-actinins, which stiffen the structure. The balance of both activities is believed to determine the flexibility of this belt, its mechanosensitivity and the tension forces exerted on the cell surface (Foley and Young, 2014; Martin and Goldstein, 2014; Murrell et al., 2015; Röper, 2015). The existence of a central apical acto-myosin network with radial contractility has also been reported (Coravos and Martin, 2016).

The α-actinin (ACTN) family comprises four members, the muscle ACTN2 and ACTN3, and the non-muscle ACTN1 and ACTN4, which are expressed in most other cell types. They share a common primary structure with a N-terminal actin-binding domain (ABD) and a C-terminal calmodulin-like domain (CAMD) separated by a central repeat of four spectrin-like domains (spectrin repeats domain; SRD). ACTN molecules form antiparallel dimers through their rigid SRD allowing for the cross-linking of actin filaments by the ABD positioned on either end. In comparison with the filamin proteins, which orthogonally cross-link actin filaments, non-muscle ACTNs form linear F-actin bundles, which increase the stiffness (Jahed et al., 2014; Stossel et al., 2001). They are believed to contribute to myosin-II-driven contractility by facilitating force transmission (Le Clainche and

[1]Université Côte d'Azur, CNRS, Institut de Pharmacologie Moléculaire et Cellulaire (IPMC), Valbonne, F-06560, France. [2]Centre de Recherche en Cancérologie de Marseille (CRCM), 'Cell Polarity, Cell Signalling and Cancer', Equipe Labellisée Ligue Contre le Cancer, Inserm U1068, Marseille, F-13009, France; CNRS, UMR7258, Marseille, F-13009, France; Institut Paoli-Calmettes, Marseille, F-13009, France; Aix-Marseille University, UM105, Marseille, F-13284, France.
*Present address: BIOASTER, Lyon, F-69007, France.

‡Author for correspondence (luton@ipmc.cnrs.fr)

J.M., 0000-0002-5861-2830; J.-P.B., 0000-0001-8418-3382; M.F., 0000-0003-1853-8661; F.L., 0000-0001-6868-4654

Received 3 August 2017; Accepted 11 December 2017

Journal of Cell Science (2018) 131, jcs209361. doi:10.1242/jcs.209361

Carlier, 2008). ACTNs also act as a mechanical linker between actin filaments and cell–cell and cell–extracellular matrix (ECM) adhesion complexes. Besides its structural roles, ACTNs could also serve to couple actin nucleation to assembly at cell–cell contacts (Tang and Brieher, 2012) and contribute to the maturation of cell–ECM focal adhesion by transmitting mechanical forces (Iskratsch et al., 2014; Jahed et al., 2014; Parsons et al., 2010; Ye et al., 2014). Both ACTN1 and ACTN4 were found at the apical acto-myosin ring in association with the AJ (Honda et al., 1998; Tang and Brieher, 2012), whereas a few studies suggested a link with the TJ (Chen et al., 2006; Geiger et al., 1979; Nakatsuji et al., 2008). Nevertheless, the repertoire of ACTN molecules associated with the various F-actin structures is poorly defined and is made even more complex by the existence of ACTN1–ACTN4 heterodimers (Foley and Young, 2013). Moreover, it is not completely clear how ACTNs are recruited to cell–cell contacts. Thus, much remains to be discovered about the role of ACTNs at the AJC as well as their role during luminogenesis.

Small G-proteins of the Rho family and their partners are key regulators in the assembly and maintenance of the PAMR. In particular, RhoA contributes to the constitution of the contractile apical acto-myosin array through the localization and activation of the formin proteins and the activation of the motor protein myosin-II by the Rho-associated coiled-coil kinase effectors ROCK1 and ROCK2 (hereafter denoted ROCK) (Arnold et al., 2017; Quiros and Nusrat, 2014; Sluysmans et al., 2017; Takeichi, 2014). Tension forces are necessary for the establishment and functioning of the AJC, as they support the changes in cell shape occurring during epithelial morphogenesis (Coravos et al., 2017; Lecuit and Yap, 2015; Takeichi, 2014). However, how contractility and its regulators are impacting epithelial cell luminogenesis is an issue of ongoing debate.

Another small G-protein that regulates the cortical cytoskeleton is the ADP ribosylation factor 6 (Arf6). It plays a pivotal role in a wide variety of cellular events including cell surface trafficking, phagocytosis, cell–cell adhesion, and tumor cell migration and invasion (D'Souza-Schorey and Chavrier, 2006; Gillingham and Munro, 2007; Jaworski, 2007; Sabe et al., 2009; Schweitzer et al., 2011). In epithelial cells, Arf6 was initially shown to regulate vesicular trafficking to the apical pole of the cell (Altschuler et al., 1999) and later to impact the turnover of the AJ (Palacios et al., 2001, 2002, 2005), the establishment of the TJ (Klein et al., 2008; Luton et al., 2004), cyst morphogenesis (Tushir et al., 2010) and HGF-induced tubulogenesis (Tushir and D'Souza-Schorey, 2007). Consistent with these observations, the exchange factor for Arf6 (EFA6; also known as PSD) was found to be enriched at the apical pole and at the TJ in fully polarized MDCK cells (Luton et al., 2004). During early epithelial polarization, EFA6 is recruited to the cell–cell contact in a manner that is dependent on E-cadherin engagement, where it contributes to the formation of the TJ by stabilizing the apical acto-myosin ring (Théard et al., 2010). Expression of EFA6B (also known as PSD4) in the mammary tumoral MCF7 cell line restored a normal glandular phenotype, with the formation of lumens delineated by TJs (Zangari et al., 2014). Conversely, knockdown of EFA6B expression drives various mammary cell lines into epithelial-to-mesenchymal transition (Zangari et al., 2014). In breast cancer patients, the loss of EF6AB expression is associated with the claudin-low subtype characterized by the loss of expression of all the TJ components and a poor prognosis (Zangari et al., 2014).

The EFA6 family consists of four isoforms (EFA6A–EFA6D; EFA6C is also known as PSD2, and EFA6D as PSD3) sharing a general structure that comprises a variable N-terminal domain, a catalytic Sec7 domain bearing the nucleotide exchange activity, a PH domain responsible for their plasma membrane localization and a conserved C-terminal region involved in actin cytoskeleton rearrangement (Derrien et al., 2002; Franco et al., 1999; Sakagami, 2008; Sironi et al., 2009). In a previous study, we found that mutations that abolish the nucleotide exchange activity or delete the C-terminal domain abrogated the stimulatory effects of EFA6, indicating that both Arf6 activation and the C-terminal domain are necessary for epithelial polarization (Luton et al., 2004). In addition, complementation experiments demonstrated a finely tuned cooperation between the two signaling pathways associated with the activated Arf6 and with the EFA6 C-terminus (Klein et al., 2008).

In this study, we aimed to determine the signaling pathway associated to EFA6 C-terminus that contributes to its action on epithelial morphogenesis. Our data showed that: (1) ACTN1 is a direct partner of EFA6A C-terminal domain, (2) EFA6A is a crucial regulator of luminogenesis for which ACTN1 is the major effector, (3) together, they stimulate the formation and enlargement of a single lumen with a proper round shape, (4) they act by regulating cortical acto-myosin contractility, and finally (5) ACTN1 is also a partner of the EFA6B isoform in the promotion of lumen formation in the mammary tumoral cells MCF7.

RESULTS

EFA6A binds directly to ACTN1

Looking for functional partners of EFA6A in epithelial cells, we performed a two-hybrid screen of an epithelial library using the C-terminus (Cter) of EFA6A as a bait, and identified ACTN1 as the major interacting protein. A similar result was found by Sakagami et al. in a previous screen using a neuronal library (Sakagami et al., 2007). A pulldown assay was used to confirm that the Cter of EFA6A could bind exogenously expressed ACTN1–GFP (Fig. 1A). We then further characterized this interaction by assessing whether the two proteins could bind directly. We found that both GST–ACTN1 and GST–ACTN4 could pulldown full-length His–EFA6A (Fig. 1B), and that the central SRD of ACTN1 binds directly to His–EFA6A (Fig. 1C). In BHK cells, GFP–EFA6A co-immunoprecipitated endogenous ACTN1 (Fig. 1D), and Myc–EFA6A re-localized the endogenous ACTN1 to F-actin-enriched lamellipodia as well as to the cell surface microspikes induced by Myc–EFA6A (Fig. 1E; Derrien et al., 2002; Macia et al., 2008). We conclude that, *in vitro*, ACTN and EFA6A can bind directly through their respective spectrin and C-terminal domains, and that, *in vivo*, EFA6A can recruit the endogenous ACTN1 to cortical F-actin structures. In agreement with our previous reports (Luton et al., 2004; Théard et al., 2010; Zangari et al., 2014), during lumen formation mRFP–EFA6A was transiently found to be enriched at the AMIS and the opened PAP before its expression at the apical surface decreased to the low level found in mature cyst (Fig. S1A). We also examined the localization of ACTN1 and ACTN4 in polarized cysts formed by MDCK cells. ACTN1–GFP was diffused within the cytoplasm and enriched at the apex of cell-cell junctions (Fig. S1A). Colocalization of ACTN1–GFP with occludin (Fig. 1Fa–a″) indicated its accumulation at the TJ. In contrast, ACTN4–GFP was not consistently observed at the TJ at above the level of the GFP control (Fig. S1A; Fig. 1Fc–c″). In addition, ACTN1–GFP was found to be enriched at the nascent lumen formed in between two cells and its surrounding TJ (Fig. 1Fb–b″), whereas ACTN4–GFP was found on the newly formed luminal membrane and also was enriched along the cell–cell contact (Fig. 1Fd–d″).

Journal of Cell Science (2018) 131, jcs209361. doi:10.1242/jcs.209361

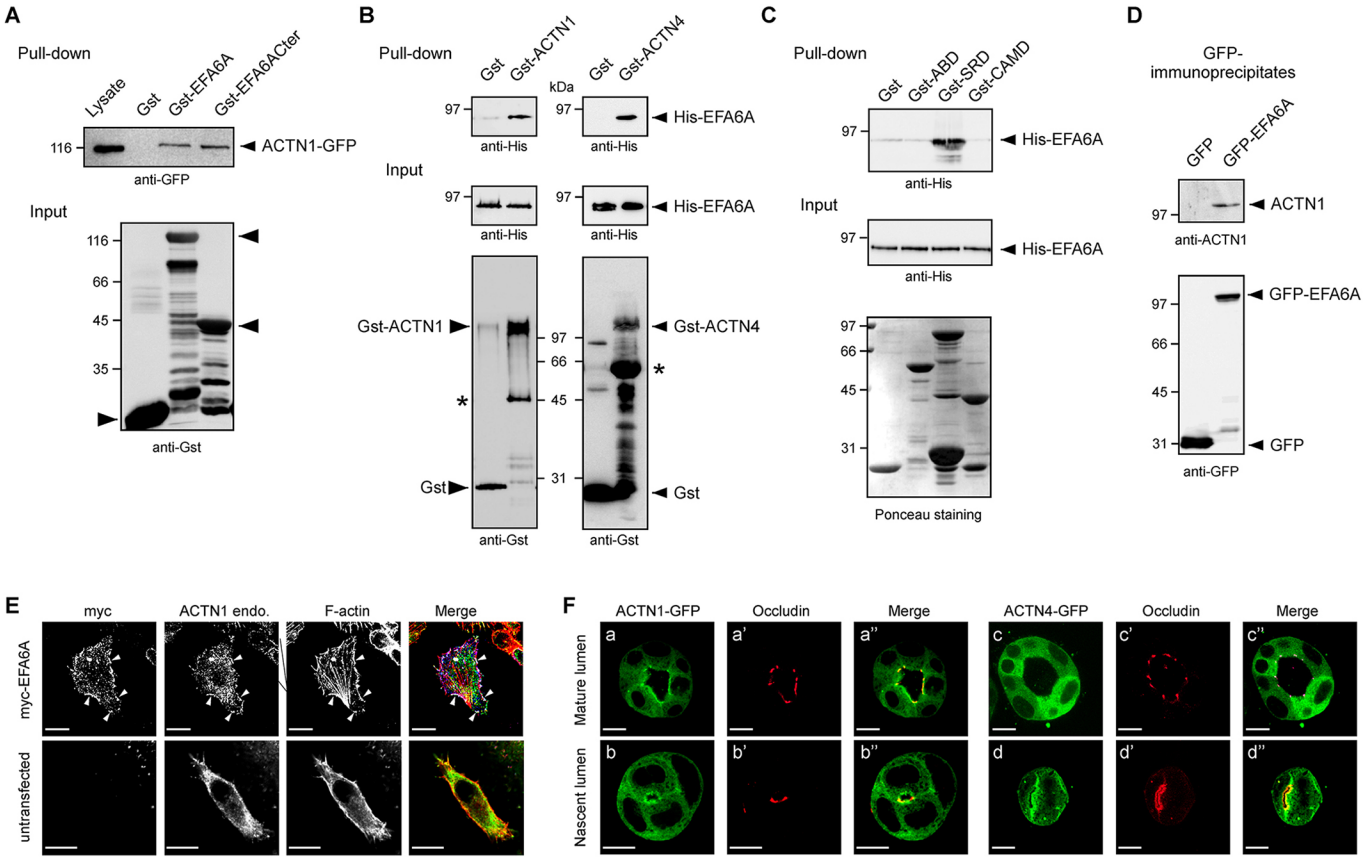

Fig. 1. EFA6A binds directly to ACTN1. (A) Lysate of MDCK cells expressing ACTN1–GFP was reacted with GST, GST–EFA6A or GST–EFA6ACter prebound to glutathione–sepharose beads. The top arrowhead points to GST–EFA6A and the bottom arrowhead to GST–EFA6ACter. (B) Purified GST, GST–ACTN1 and GST–ACTN4 prebound to glutathione–sepharose beads were reacted with purified (6xHis)–EFA6A. The asterisk highlights a main purification contaminant. (C) Purified GST, GST–ABD, GST–SRD and GST–CAMD (fragments of ACTN1) prebound to glutathione–sepharose beads were reacted with purified (6xHis)-EFA6A. In A–C, the input or whole lysate and bound proteins were analyzed by immunoblotting with the indicated antibodies. (D) GFP or GFP–EFA6A expressed in BHK cells were immunoprecipitated using an anti-GFP antibody and the co-precipitation of endogenous ACTN1 was assessed by immunoblotting. (E) BHK cells expressing or not expressing Myc–EFA6A were processed for immunofluorescence and stained for Myc (blue), F-actin (red) and the endogenous ACTN1 (ACTN1 endo., green). Arrowheads point to EFA6A-induced lamellipodia where the endogenous ACTN1 is recruited. (F) MDCK cells expressing ACTN1–GFP (green; a–b″) or ACTN4–GFP (green; c–d″) were processed for immunofluorescence to label the endogenous occludin (red) in mature or nascent lumens. Scale bars: 10 µm.

Later, in mature cysts, ACTN4–GFP appeared to be more enriched in AJs stained for E-cadherin (Fig. S1B). Given the enrichment of ACTN1 at the TJ, we focused our study on the importance of its role as an effector of EFA6.

EFA6A recruits ACTN1 in a regulated manner

EFA6A and ACTN1 are cortical actin regulators and both partially localize to the TJ in polarized epithelial cells; we thus investigated the mechanism of their direct interaction. ACTN1 could serve as a receptor to recruit EFA6A to the TJ. However, EFA6A localization to the plasma membrane was shown to rely on its phosphatidylinositol 4,5-bisphosphate (PIP2)-specific PH domain and its capacity to bind to F-actin (Macia et al., 2008). Furthermore, the EFA6A mutant deleted of its C-terminus, which no longer binds ACTN1, has been shown to localize at the plasma membrane in a similar manner to the full-length protein (Franco et al., 1999; Macia et al., 2008). In contrast, as shown above (Fig. 1E) ACTN1 was re-localized to Myc–EFA6A-induced membrane ruffles, suggesting that ACTN1 can be used as an effector of EFA6A in order to remodel the cortical actin cytoskeleton.

To further analyze the binding of ACTN1 to EFA6A and its functional properties in living cells, we ectopically expressed EFA6A away from the plasma membrane. We fused EFA6A to the mitochondrial-targeting peptide ActA and determined whether EFA6A–ActA was capable of re-localizing the endogenous ACTN1 to the outer membrane of mitochondria, from which it is normally absent. Since ACTN1 binds to the C-terminal domain of EFA6A, we first studied the EFA6ACter fused to mRFP and ActA (named hereafter EFA6ACter–mRFP–ActA). As previously observed by others, depending on the expression rate and construct used, in cells transfected with ActA chimeras the mitochondrial network tended to aggregate around the nucleus (Bubeck et al., 1997; Moeller et al., 2004; Reinhard et al., 1999; Zhang et al., 2009). Nevertheless, all constructs localized to the mitochondria as assessed by monitoring colocalization with the mitochondrial protein Hsp60 (also known as HSPD1) (Fig. S2A). When expressed in BHK cells, EFA6ACter–mRFP–ActA localized to the mitochondria (Fig. S2A) and recruited endogenous ACTN1 (Fig. 2A; magnification in Fig. S2B). In contrast, the control mRFP–ActA construct, which also localized to the mitochondria (Fig. S2A), did not recruit ACTN1 (Fig. 2A). Interestingly, the full-length EFA6A–mRFP–ActA localized to the mitochondria (Fig. S2A) but did not re-localize ACTN1 (Fig. 2A). This observation suggests that the Cter was not available for ACTN1 binding in the full-length EFA6A. Our previous work indicates that EFA6A exists in a closed conformation where the Cter is folded

Journal of Cell Science (2018) 131, jcs209361. doi:10.1242/jcs.209361

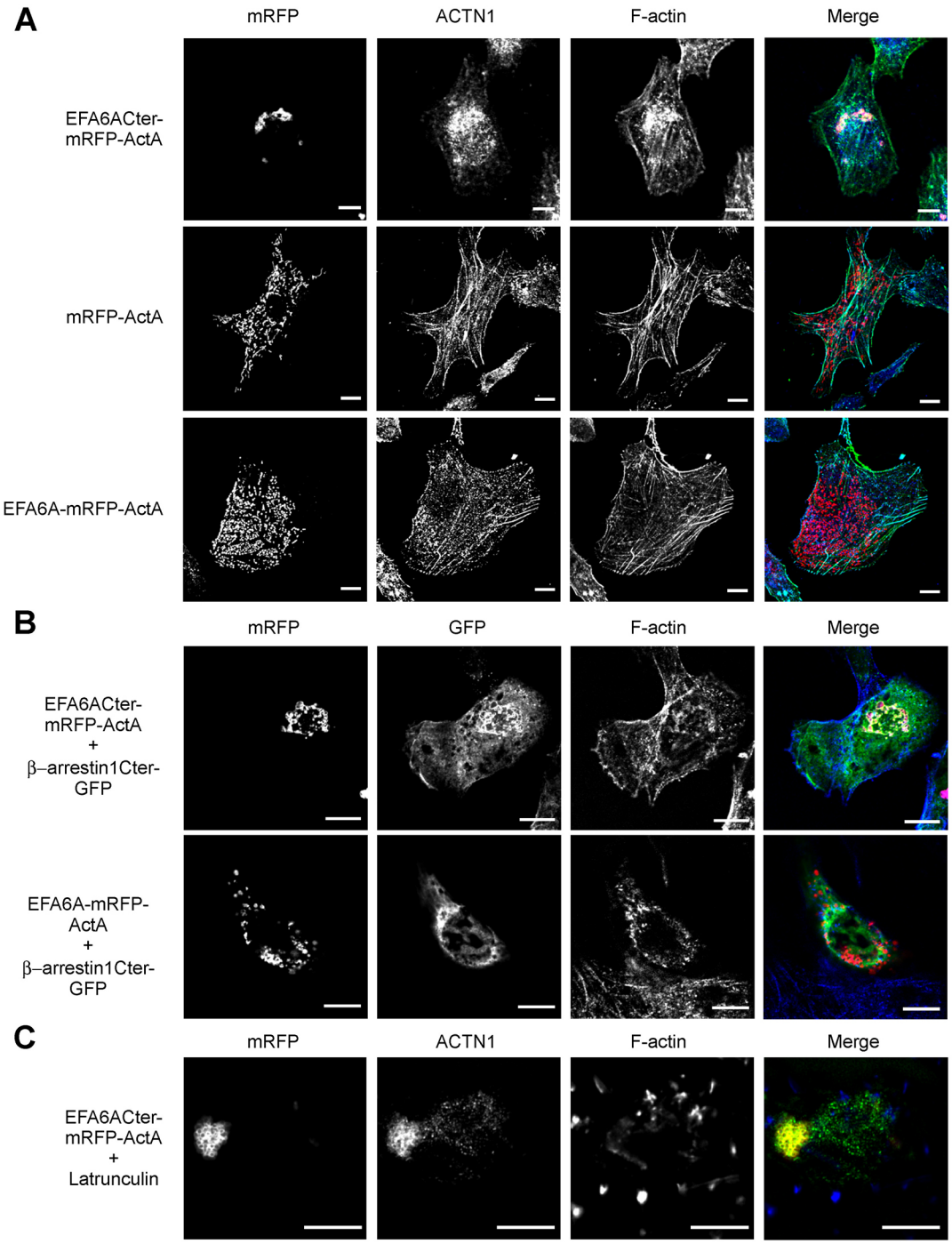

Fig. 2. EFA6A recruits ACTN1 in a regulated manner. (A) BHK cells expressing EFA6ACter–mRFP–ActA, mRFP–ActA and EFA6A–mRFP–ActA were processed for immunofluorescence to label the endogenous ACTN1 and F-actin. In merge images, mRFP is colored red, ACTN1 blue and F-actin green. (B) BHK cells co-expressing β-arrestin1Cter–GFP (green) with EFA6ACter–mRFP–ActA (red) or with the full-length EFA6A–mRFP–ActA (red) were processed for immunofluorescence to label the endogenous F-actin (blue). (C) BHK cells expressing EFA6ACter–mRFP–ActA were exposed to Latrunculin A (2 µM) for 2 h. The cells were processed for immunofluorescence to label the endogenous ACTN1 (green) and F-actin (blue). Scale bars: 10 µm.

back onto the PH domain, preventing its association with the C-terminus of β-arrestin1 (denoted β-arrestin1Cter), another EFA6ACter ligand (Macia et al., 2012). To test whether the EFA6A–mRFP–ActA was in a locked conformation, we co-expressed β-arrestin1Cter–GFP with EFA6ACter–mRFP–ActA or the full-length EFA6A–mRFP–ActA constructs. Similar to what was observed with ACTN1, β-arrestin1Cter–GFP could only bind to EFA6ACter–mRFP–ActA (Fig. 2B) indicating that the binding of ACTN1 to EFA6A is regulated, and requires the release of its C-terminal domain.

Some F-actin staining was observed colocalized together with EFA6ACter–mRFP–ActA and the endogenous ACTN1 at the mitochondria (Fig. 2A; magnification in Fig. S2B). When the cells were treated with Latrunculin A, F-actin was absent from the mitochondria whereas the endogenous ACTN1 was still efficiently recruited by EFA6Cter–ActA (Fig. 2C). Thus, independently of the

Journal of Cell Science (2018) 131, jcs209361. doi:10.1242/jcs.209361

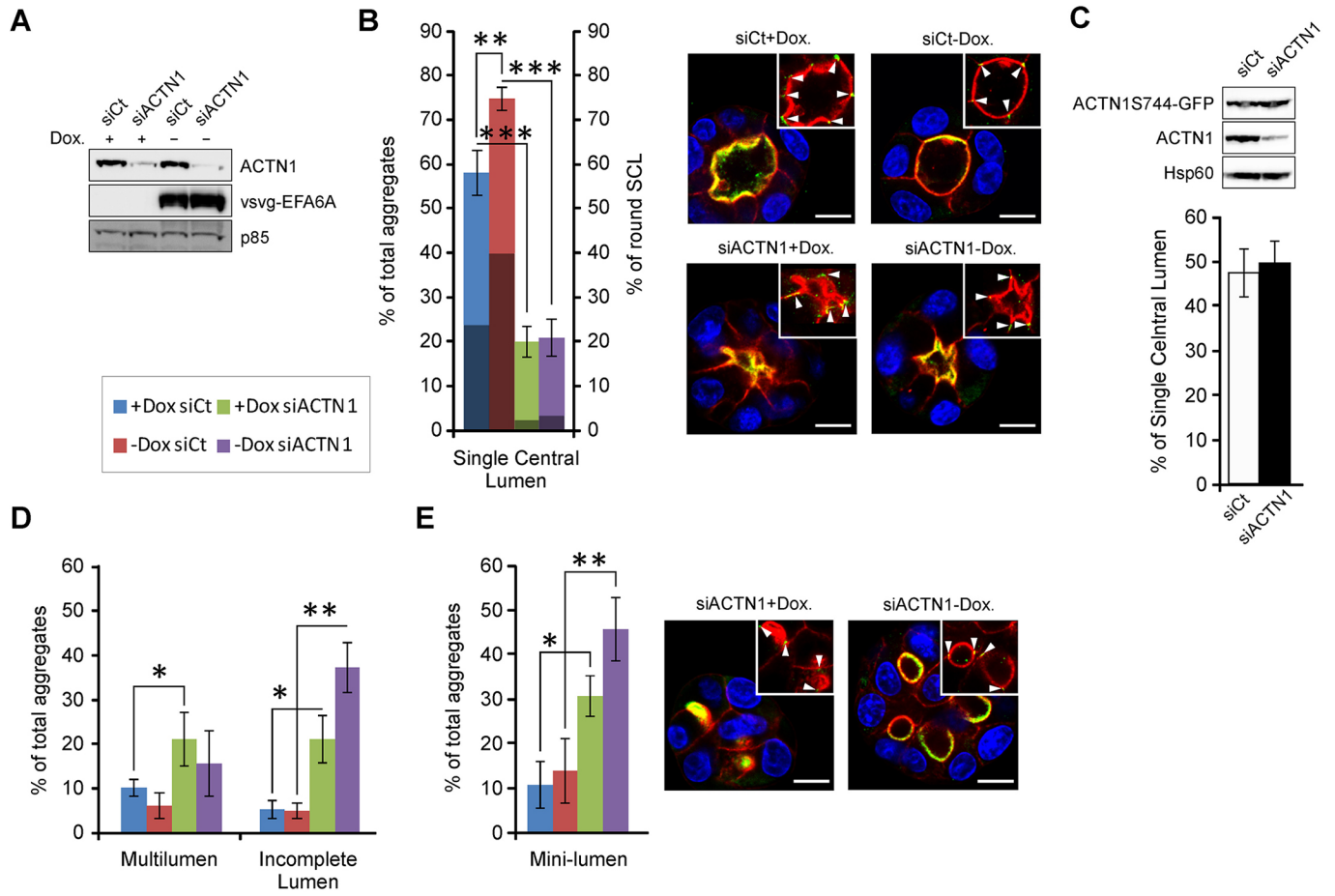

Fig. 3. Depletion of ACTN1 inhibits normal EFA6A-induced luminogenesis. (A) MDCK cells expressing inducible VSV-G–EFA6A were transfected with siRNA directed against ACTN1 (siACTN1; #2225) or with control siRNA (siCt), and were grown without or with doxycycline (Dox) to induce or not the expression of VSV-G–EFA6A, respectively. At 48 h post transfection, the cells were solubilized in SDS lysis buffer and the expression of the indicated proteins was analyzed by immunoblotting. The p85 regulatory subunit of PI3K served as a loading control. (B) Left, quantification of the percentage of cell aggregates with a SCL (left *y*-axis). Shaded areas indicate the percentage of those SCL aggregates with a round lumen (right *y*-axis). Results are mean±s.d., *n*=5. Right, representative images of the four cell types labeled for the nuclei (blue), apical marker PDX (green) and F-actin (red) are shown. The insets display an image of the same lumens stained for F-actin (red) and the TJ marker occludin (green). Arrowheads point to the TJs. (C) MDCK cells expressing ACTN1S744–GFP were transfected with siCt or siACTN1 (#2225). Top panel, the cells were solubilized in SDS lysis buffer and the expression of the indicated proteins analyzed by immunoblotting. Hsp60 served as a loading control. Bottom panel, quantification of the percentage of aggregates with a SCL. No significant difference was measured. Results are mean±s.d., *n*=3. (D) Quantification of the percentage of aggregates with multilumens or incomplete lumens for the indicated conditions. Results are mean±s.d., *n*=5. (E) Quantification of the percentage of aggregates with mini-lumens for the indicated conditions. Representative images of cells depleted in ACTN1, and expressing or not expressing VSV-G–EFA6A, labeled for the nuclei (blue), the apical marker PDX (green) and F-actin (red). The insets display an image of the same mini-lumens stained for F-actin (red) and the TJ marker occludin (green). Arrowheads point to the TJ. **P*≤0.05; ***P*≤0.01; ****P*≤0.001 (Student's *t*-test). Scale bars: 10 µm.

presence of F-actin, EFA6A can directly recruit ACTN1, which in turn might function as an effector to organize EFA6A-regulated actin-based structures.

Depletion of ACTN1 inhibits normal EFA6A-induced luminogenesis

We have previously shown that expression of EFA6A tagged with the G glycoprotein of the vesicular stomatitis virus (VSV-G) (VSV-G–EFA6A) stimulates apical polarity development and TJ formation in MDCK cells (Klein et al., 2008; Luton et al., 2004). To assess the role of ACTN1 as an effector of EFA6A, we analyzed the effects of its downregulation in cells grown in a 3D-culture system in Matrigel. Several siRNAs against ACTN1 were tested for their efficiency to downregulate its expression (Fig. S3A). ACTN1 knockdown was carried out in MDCK cells in which the expression of VSV-G–EFA6A is under the control of the tetracycline (Dox)-repressible transactivator (hereafter denoted MDCK-VSV-G–EFA6A cells) (Luton et al., 2004). Fig. 3A is a representative immunoblot analysis of ACTN1 depletion and VSV-G–EFA6A expression in the presence or absence of doxycycline.

We first examined whether EFA6A overexpression stimulated epithelial polarity in MDCK cells grown in Matrigel over 3 days. Cysts of homogenous size (from 4 to 15 cells) were analyzed for the formation of one or multiple lumens and for their shape. They were also characterized for extension and expansion. Extension refers to the opening of the lumen to all the cells of the aggregates, while expansion refers to the enlargement of the luminal space. Upon VSV-G–EFA6A expression (−Dox) we observed an increase in the formation of cysts displaying a single central lumen (SCL). In addition, the luminal space became more round with an almost doubling (from 23% to 40%) of the SCL, with it displaying a round shape upon VSV-G–EFA6A expression (Fig. 3B, shaded bars and upper right panel). In contrast, depletion of ACTN1 in control conditions (+Dox) reduced the number of cysts with a SCL and

Journal of Cell Science (2018) 131, jcs209361. doi:10.1242/jcs.209361

severely altered the shape of the lumen such that the lumens adopted an 'octopus-like' shape with a small central opening from which closed or barely opened luminal extensions reached in between the cells (Fig. 3B, shaded bars and lower left panel). Depletion of ACTN1 in cells expressing VSV-G–EFA6A also impaired enlargement of the lumens, although the opening was more visible (Fig. 3B, shaded bars and bottom right panel). Thus, ACTN1 is required for the stimulatory effects found for EFA6A on SCL formation and on the rounding of the luminal space of multicellular cysts. However, in all conditions, the cells remained well polarized as indicated by the correct localization of the apical podocalyxin (PDX; also known as PODXL) and basolateral (E-cadherin) markers (Fig. S3B), and by the basal positioning of the nuclei, the general F-actin organization and the apical assembly of the TJ (Fig. 3B). To confirm that the phenotypes induced by the siRNA against ACTN1 (siACTN1) were due to ACTN1 depletion we carried out a rescue experiment. MDCK cells expressing an ACTN1–GFP which is insensitive to the siACTN1 (ACTN1S744–GFP) did not display any defect in lumen formation upon depletion of the endogenous ACTN1 (Fig. 3C).

The loss of cysts with SCLs in the ACTN1-depleted cells was counterbalanced by an increase of cell aggregates with multiple lumens and others with incomplete extension to all of the cells (Fig. 3D, see Materials and Methods). In both cases, the lumens displayed the distorted octopus-like shape. The extension defect was further reflected by a strong increase in the number of aggregates displaying multiple lumens that only opened in between two cells (hereafter called mini-lumens) that were often blocked at the PAP stage with no visible opening (Fig. 3E), which suggests that ACTN1 depletion might favor the early formation of an initial lumen. VSV-G–EFA6A expression did not significantly alter the phenotypic changes imposed upon ACTN1-depletion; however, it stimulated the enlargement and rounding of the mini-lumens blocked at the two-cell stage (Fig. 3E, right panel). Thus, as opposed to what is seen for mature lumens, EFA6A can stimulate the volumetric enlargement of nascent mini-lumens in an ACTN1-independent manner. Taken together, these observations suggest that ACTN1 is dispensable for the formation of the initial lumen in between two cells but is required later on for its extension and enlargement (see Discussion section for further comments). In summary, depletion of ACTN1 blocked both the effects of VSV-G–EFA6A on luminogenesis, that is, the formation of fully extended SCL and its expansion as regular round lumen. This suggests that ACTN1 acts as an effector downstream of EFA6A that is important for luminogenesis.

ACTN1 acts as an effector of EFA6A to promote normal luminogenesis

If EFA6A controls luminogenesis and ACTN1 acts as an effector, then EFA6A depletion should hamper luminogenesis, and when combined with ACTN1 depletion there should have no additional effect. MDCK-VSV-G–EFA6A cells grown in the absence or presence of doxycycline were submitted to siRNA against EFA6A (siEFA6A)-, siACTN1- or simultaneous siEFA6A- and siACTN1-mediated depletion. The efficient knockdown of the indicated proteins and the induction of the expression of VSV-G–EFA6A were analyzed by immunoblotting (Fig. 4A; Fig. S4).

Depletion of the endogenous EFA6A was accompanied by a reduction in the amount of cell aggregates with a SCL demonstrating that EFA6A is required for luminogenesis (Fig. 4B). Expression of the exogenous human VSV-G–EFA6A, which is insensitive to the canine-specific siRNA, rescued the normal phenotype, thus controlling for the specificity of EFA6A knockdown (Fig. 4B). As shown in Fig. 3, ACTN1 depletion hampered luminogenesis and blocked the VSV-G–EFA6A stimulation. However, ACTN1 depletion did not have any additional effect when the endogenous EFA6A was knocked down (Fig. 4B). In addition, the exogenous expression of VSV-G–EFA6A in the double knockdown cells could not rescue the normal phenotype (Fig. 4B). In addition, we analyzed the consequences on the lumen formation of expressing a mutant of EFA6A deleted of its C-terminus (EFA6AΔC), which contains the ACTN1-binding site. Expression of VSV-G–EFA6AΔC impaired normal luminogenesis and caused the formation of lumens with an octopus-like shape (Fig. 4C). Although the C-terminus of EFA6A likely interacts with other molecules, it is important to note that its truncation generated lumens with shapes that were similar to those observed in ACTN1-depleted cells. Taken together, these observations indicate that EFA6A mediates luminogenesis in MDCK cells and that ACTN1 is a crucial effector for this process.

ACTN1 is an effector of EFA6B for luminogenesis induction in MCF7 breast cancer cells

We have reported that the EFA6B isoform is an antagonist of breast cancer development (Zangari et al., 2014). Tumoral MCF7 cells grown in 3D-culture systems form compact aggregates with no lumen (Han et al., 2010; Kenny et al., 2007). The exogenous expression of VSV-G–EFA6B in the tumoral MCF7 cells restores an epithelial phenotype characterized by the appearance of aggregates with extended lumens (although not often a SCL), delineated by functional TJs (Zangari et al., 2014). Thus, we asked whether ACTN1 was required downstream of EFA6B to contribute to luminogenesis in MCF7 cells.

We first verified that ACTN1 could also bind to the EFA6B isoform (Fig. S5). Next, we analyzed the effect of ACTN1 depletion in both control MCF7 and MCF7-VSV-G–EFA6B cells grown in Matrigel. An immunoblot analysis demonstrated the efficient knockdown of ACTN1 in both cell lines (Fig. 5A). We quantified the number of aggregates with extended lumens opened to at least four cells, as opposed to mini-lumens opened in between only two cells. As previously reported, MCF7 control cells do not form cysts with lumens (Han et al., 2010; Kenny et al., 2007; Zangari et al., 2014), whereas exogenous expression of VSV-G–EFA6B induced the formation of cysts with extended lumens (Fig. 5B; Zangari et al., 2014). We observed that ACTN1 depletion blocked the formation of extended lumens induced by EFA6B indicating that, in MCF7 cells, ACTN1 is also a crucial effector of EFA6B-induced lumen formation (Fig. 5B). In addition, although control MCF7 cell aggregates did not form extended lumens, in ∼20% of the aggregates one or several mini-lumens were observed (Fig. 5C,D). Upon ACTN1 depletion, the number of these mini-lumens increased in both the VSV-G–EFA6B-expressing and non-expressing MCF7 cell lines. However, in VSV-G–EFA6B-expressing cells aggregates the luminal space was enlarged while in MCF7 controls cells the mini-lumens were seen as PAPs (Fig. 5C,D). Thus, similar to what we had observed in MDCK cells, ACTN1 depletion facilitates the initial lumen formation in between two cells but then hampers both extension and enlargement.

EFA6A and ACTN1 control apical contractility contributing to luminogenesis

The PAMR and ventral stress fibers (SFs) are sarcomere-like actin-based structures capable of contractility that have been implicated in epithelial morphogenesis. Contractile actin bundles are formed by aligned fibers cross-linked by a periodic distribution of ACTNs that alternates with myosin-II (Burridge and Wittchen, 2013; Sluysmans

Journal of Cell Science (2018) 131, jcs209361. doi:10.1242/jcs.209361

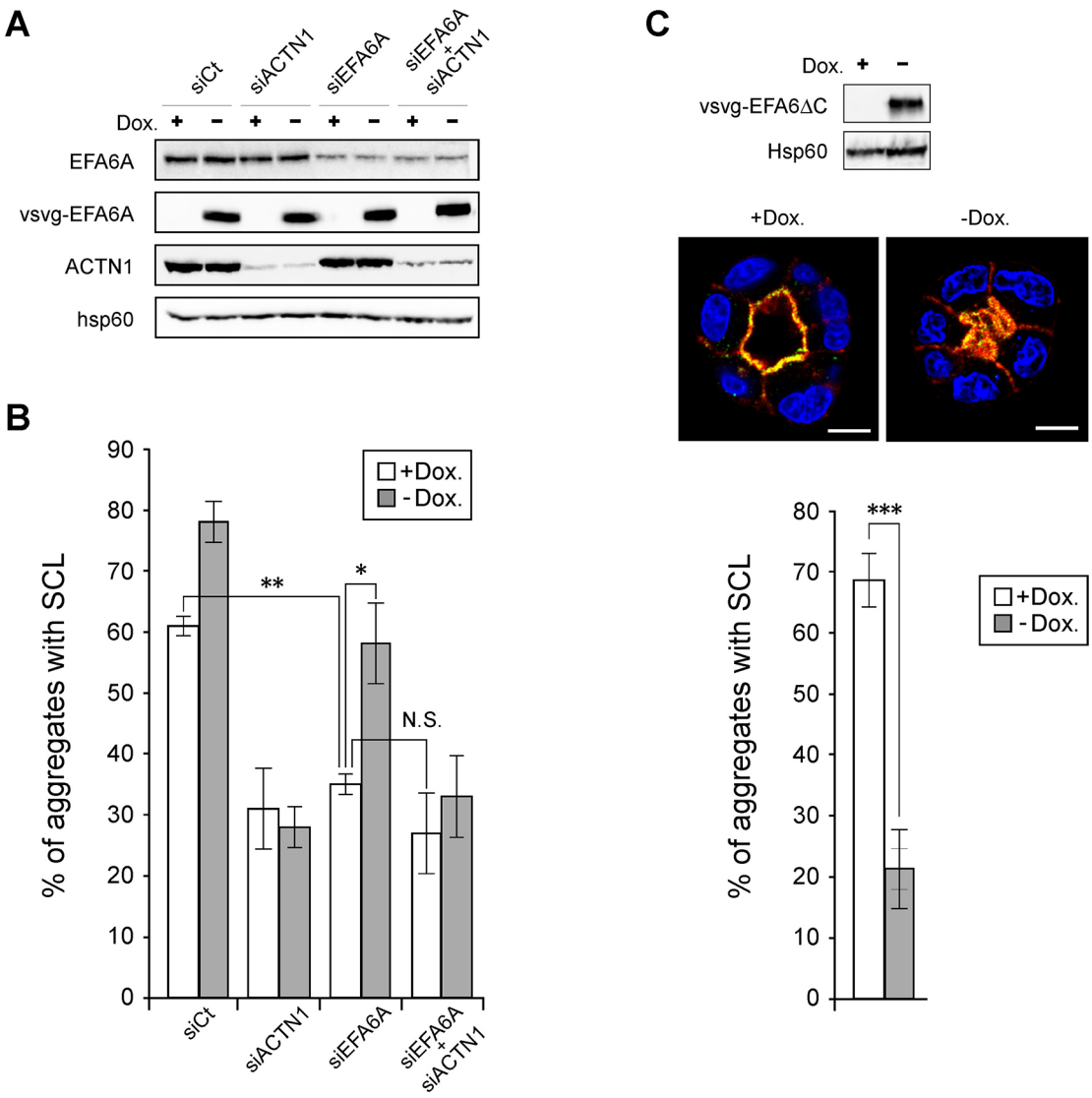

Fig. 4. ACTN1 acts as an effector of EFA6A to promote normal luminogenesis. (A) MDCK cells expressing inducible VSV-G–EFA6A were transfected with siRNA control (siCt), siRNA directed against ACTN1 (siACTN1; #2225) or EFA6A (siEFA6A; #2661), or both siACTN1 and siEFA6A, and then grown without or with doxycycline (Dox) to induce or not the expression of VSV-G–EFA6A, respectively. At 48 h post transfection the cells were solubilized in SDS lysis buffer and the expression of the indicated proteins analyzed by immunoblotting. Hsp60 served as a loading control. (B) Quantification of the percentage of cell aggregates with a SCL. Results are mean±s.d., n=4. (C) MDCK cells expressing inducible VSV-G–EFA6AΔC were grown with or without Dox. Top panel, at 48 h post transfection the cells were solubilized in SDS lysis buffer and the expression of VSV-G–EFA6AΔC analyzed by immunoblotting. Hsp60 served as a loading control. Middle panel, representative images of cell aggregates grown with or without Dox labeled for the nuclei (blue), apical marker PDX (green) and F-actin (red). Bottom panel. quantification of the percentage of cell aggregates with a SCL. Results are mean±s.d., n=3. *P≤0.05; **P≤0.01; ***P≤0.001; N.S., not significant (Student's t-test). Scale bars: 10 µm.

et al., 2017). RhoA and its effectors (ROCK and mDia1) have been recognized as major regulators of the contractile properties of the acto-myosin cytoskeletons (Arnold et al., 2017; Quiros and Nusrat, 2014; Sluysmans et al., 2017; Takeichi, 2014). Thus, we tested the possibility that EFA6A and ACTN1 regulate luminogenesis by contributing to the PAMR contractility. First, we used an antibody directed against the phosphorylated regulatory myosin light chain 2 (pMLC, also known as MYL2) as a proxy to evaluate the tension forces in response to modulating EFA6A and ACTN1 expression. Fig. 6B shows a representative immunoblot analysis of ACTN1 depletion and VSV-G–EFA6A expression in the presence or absence of doxycycline. In control cells, the pMLC staining appeared as small intracellular dots, as well as larger dots located in proximity to the apical membrane. Under conditions of EFA6A or ACTN1 depletion, this apical staining disappeared and the pMLC distribution became more diffuse. Upon VSV-G–EFA6A expression the proportion of apical pMLC was increased and its staining was evenly distributed all around the luminal cortex. In ACTN1-depleted cells, the VSV-G–EFA6A-induced apical accumulation of pMLC was abrogated (Fig. 6A). These results suggest that EFA6A can modulate the apical tension forces in an ACTN1-dependent manner.

We investigated the contribution of ACTN1 by first analyzing the effect of its depletion on the RhoA-stimulated ventral SFs in MDCK cells by expressing the N-terminal Myc-tagged constitutively active mutant of RhoA (Myc–RhoAV14) under the control of the inducible Tet-off system. The levels of expression of the proteins in different conditions were analyzed by immunoblotting (Fig. 6C). We monitored the Myc–RhoAV14-induced SF contractility by immunofluorescence. We looked at the F-actin organization and the

Journal of Cell Science (2018) 131, jcs209361. doi:10.1242/jcs.209361

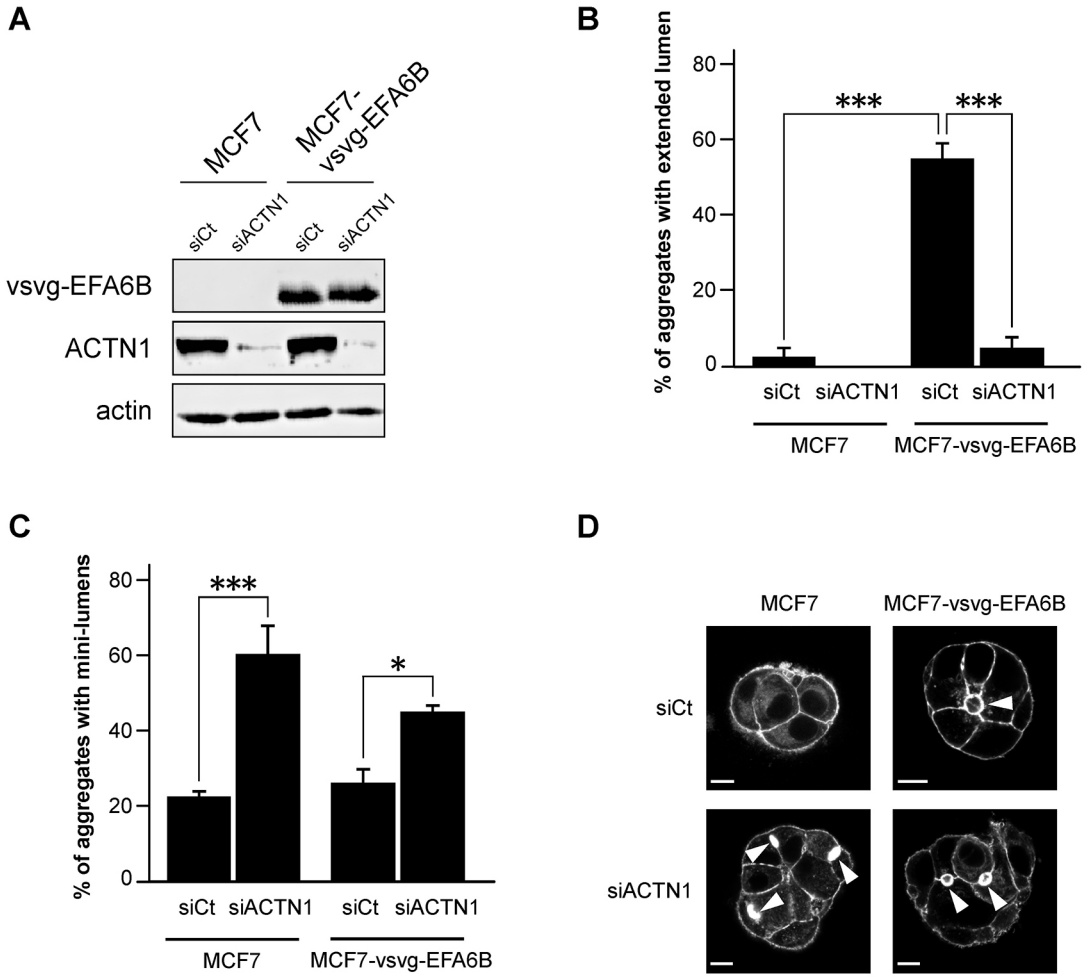

Fig. 5. ACTN1 is an effector of EFA6B that acts to induce luminogenesis in the MCF7 breast cancer cell line. (A) Control and VSV-G–EFA6B-expressing MCF7 cells were transfected with siRNA control (siCt) or siRNA directed against ACTN1 (siACTN1). At 48 h post transfection the cells were solubilized in SDS lysis buffer and the expression of the indicated proteins analyzed by immunoblotting. Actin served as a loading control. (B) Quantification of the percentage of the indicated cell aggregates with extended lumens. (C) Quantification of the percentage of the indicated cell aggregates with mini-lumens. Results in B and C are mean±s.d., n=3. *P≤0.05; ***P≤0.001 (Student's t-test). (D) Representative images of cells depleted or not for ACTN1 and expressing or not expressing VSV-G–EFA6B. The cell aggregates were processed for immunofluorescence by labeling cytoskeletal F-actin with fluorescent phalloidin. Arrowheads point to PAPs. Scale bars: 10 µm.

contractility status by following the distribution of pMLC and paxillin, a marker of the focal adhesions (Fig. 6D). As expected, the expression of Myc–RhoAV14 (−Dox) stimulated the formation of SFs that appeared as thick bundles of parallel F-actin going across the whole cell cluster (Fig. 6Db). In Myc–RhoAV14-expressing cells, pMLC was redistributed all along the SFs (Fig. 6Db′) while in control cells pMLC was enriched at the periphery of the cell cluster and excluded from cell–cell contacts (Fig. 6Da′). Concomitantly, paxillin was re-localized to the periphery of the cell cluster mostly decorating the focal adhesions at the extremity of the SF (Fig. 6Db″). As previously observed by others (Oakes et al., 2012), depletion of ACTN1 in control cells (+Dox) led to the loss of bundles or shortening of radial F-actin bundles resembling transverse arcs (Fig. 6Dc). These structures were stained for pMLC, which remained absent from cell–cell contacts (Fig. 6Dc′). The paxillin signal increased but was still homogeneously distributed within each cell of the cluster similar to what was seen in control cells (Fig. 6Dc″). Depletion of ACTN1 blocked the effects of Myc–RhoAV14, leading to cells displaying a phenotype that was comparable to that of the control cells with respect to all three markers (Fig. 6Dd–d″). We conclude that ACTN1 can balance the contractility status of RhoA-dependent SFs in MDCK cells.

Interfering with the RhoA–ROCK–myosin-II contractility pathway has been shown to alter luminogenesis in MDCK cells (Ferrari et al., 2008; Kim et al., 2015; Rodríguez-Fraticelli et al., 2012). In particular, under permissive conditions, the constitutively active RhoAV14 mutant blocks the initial step of lumen formation (Ferrari et al., 2008). We thus asked whether ACTN1 depletion could prevent the Myc–RhoAV14 inhibitory effect on luminogenesis. In our 3D cell culture conditions, Myc–RhoAV14 expression abrogated lumen formation. The cells became round and loosely attached, forming aggregates almost exclusively without lumens and that displayed an inverted polarity, as judged by the peripheral localization of the apical PDX marker (Fig. 6E,F). ACTN1 depletion partially rescued the formation of lumens (Fig. 6E). We observed aggregates with multilumens or incomplete lumen formation, essentially as mini-lumens (Fig. 6E). The cells adopted a more cuboidal shape and formed more-compact aggregates (Fig. 6F). These results suggest that the knockdown of ACTN1 acts to reduce the strong

Journal of Cell Science (2018) 131, jcs209361. doi:10.1242/jcs.209361

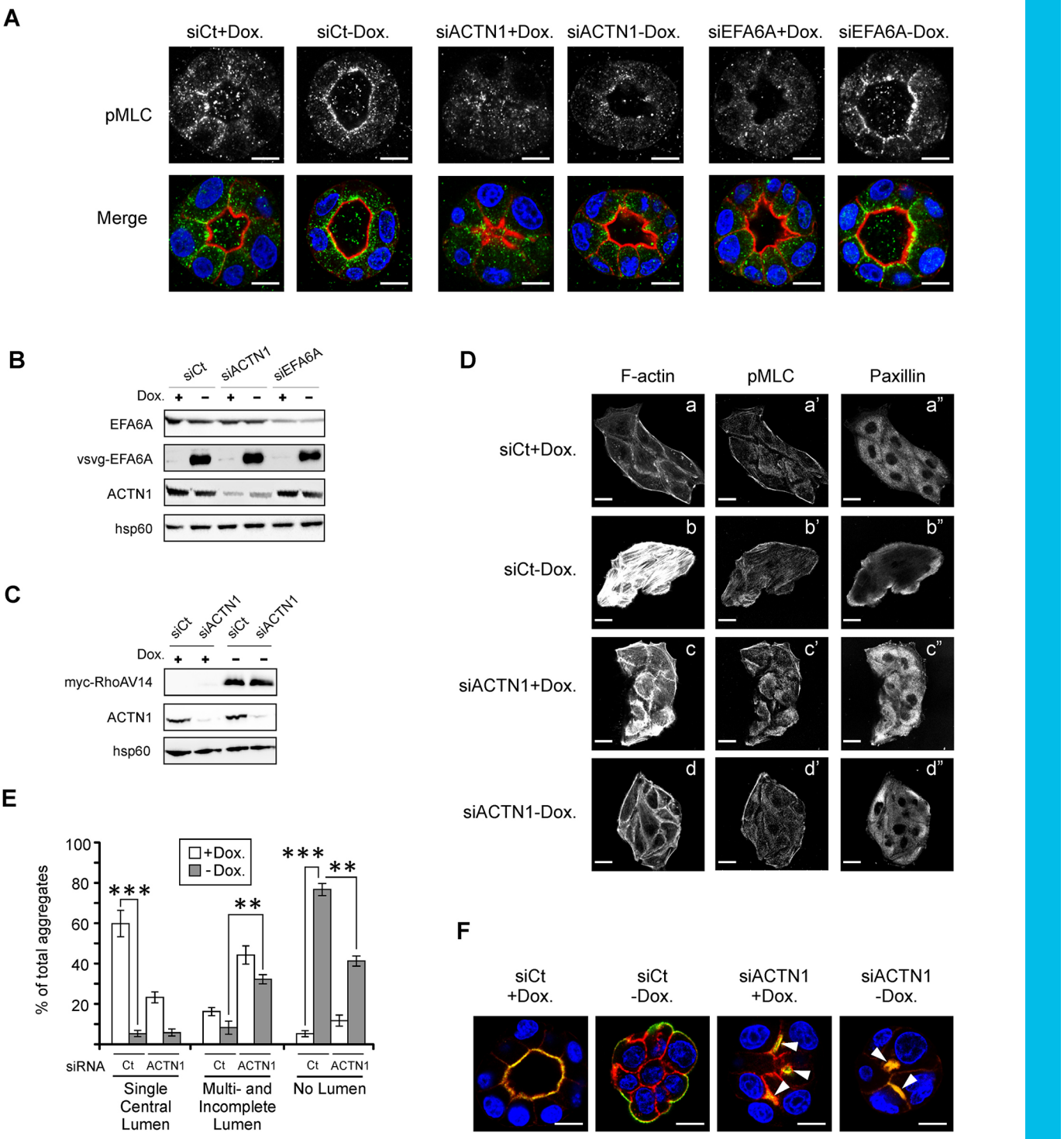

Fig. 6. EFA6A and ACTN1 control apical contractility, thereby contributing to luminogenesis. (A,B) MDCK cells expressing inducible VSV-G–EFA6A were transfected with siRNA control (siCt), or siRNA directed against ACTN1 (siACTN1; #2225) or EFA6A (siEFA6A; #2661) and then grown without or with doxycycline (Dox) to induce or not the expression of VSV-G–EFA6A, respectively. (A) Representative images of the aggregates labeled for pMLC, F-actin and the nuclei. Top panels, pMLC staining alone. Bottom panels show the corresponding merged images; pMLC is colored in green, F-actin in red and the nuclei in blue. Scale bars: 10 µm. (B) At 48 h post transfection the cells were solubilized in SDS lysis buffer and the expression of the indicated proteins analyzed by immunoblotting. Hsp60 served as a loading control. (C) MDCK cells expressing inducible Myc–RhoAV14 were transfected with siCt or siACTN1 (#2225) and grown with or without doxycycline. At 48 h post transfection the cells were solubilized in SDS lysis buffer and the expression of the indicated proteins was analyzed by immunoblotting. Hsp60 served as a loading control. (D) MDCK cells expressing inducible Myc–RhoAV14 were transfected with siCt or siACTN1 (#2225) and grown on coverslips with or without doxycycline. At 48 h post transfection the cells were processed for immunofluorescence and labeled for F-actin (a–d), pMLC (a′–d′) and the focal adhesion protein paxillin (a″–d″). Scale bars: 20 µm. (E) MDCK cells expressing inducible Myc-RhoAV14 were transfected with siCt or siACTN1 (#2225), and grown with or without doxycycline in Matrigel. Quantification of the indicated cell aggregates for SCLs, multilumens and incomplete lumens or no lumen is reported in the bar graph. Results are mean±s.d., n=3. **$P\leq0.01$; ***$P\leq0.001$ (Student's t-test). (F) Representative images MDCK cells with inducible Myc–RhoAV14 depleted or not for ACTN1 (#2225) and grown for 4 days in Matrigel with or without doxycycline. The cell aggregates were processed for immunofluorescence and labeled for the nuclei (blue), the apical marker PDX (green) and the F-actin (red). Arrowheads point to PAPs and mini-lumens. Scale bars: 10 µm.

contractility imposed by Myc–RhoAV14, thus allowing the initiation of lumen formation. This is in agreement with previous studies that show that reduction of the myosin-II contractility stimulates the initial early step of lumen opening at the two-cell stage (Ferrari et al., 2008; Rodríguez-Fraticelli et al., 2012). However, the extension and enlargement of the lumens, which we demonstrate to be dependent on ACTN1, were both still compromised upon reduction of contractility induced by ACTN1 depletion. Thus, our findings support a model whereby the initial stage of the lumen formation is facilitated by the absence of ACTN1, followed by lumen maturation, which is ACTN1 dependent.

Taken together, our data suggest that EFA6A and its effector ACTN1 contribute to SCL formation through the regulation of the cell surface tension forces within the cell aggregate.

DISCUSSION

In this study, we aimed to define the role of EFA6, a regulator of epithelial polarization, in lumen formation by using a 3D epithelial cell culture system. Given the importance of the reorganization of the actin cytoskeleton during cystogenesis, we were particularly interested in deciphering the signaling pathway associated with the EFA6 C-terminal domain that is capable of remodeling the cortical actin independently of EFA6 GEF activity.

Searching for partners of EFA6ACter, we find that EFA6A binds directly to the non-muscular ACTN member ACTN1. We characterized this interaction in living cells by using a mitochondrial-targeting system, and observed that it is likely regulated by the structural conformation of the EFA6A C-terminus. This observation confirms our previous results obtained with another EFA6Cter ligand, β-arrestin1 (Macia et al., 2012), and implies the existence of a common regulatory mechanism whereby binding to EFA6ACter requires an opening signal. A possible candidate for mediating this signal is Arf6-GTP, the product of EFA6A Sec7-dependent nucleotide exchange activity. ARNO (also known as CYTH2), another Sec7 family guanine nucleotide exchange factor for Arf1, was shown to adopt an auto-inhibited conformation where its short C-terminus downstream of the PH domain interferes with the catalytic Sec7 domain (DiNitto et al., 2007). Arf6-GTP binds to the PH domain of ARNO and stimulates, in synergy with plasma membrane lipids, the nucleotide exchange activity of ARNO on Arf1 (Cohen et al., 2007b; Stalder et al., 2011). We found that Arf6-GTP binds to the PH-C-terminal region of EFA6 (Padovani et al., 2014). Thus, by analogy with ARNO, one could speculate that Arf6-GTP, by binding to the PH domain of EFA6, could release the C-terminus and allow for ACTN1 binding.

We had previously reported that EFA6A is present at and regulates the TJ (Luton et al., 2004; Théard et al., 2010), where we now find ACTN1. Our results support the hypothesis that it is EFA6A that recruits ACTN1. The re-localization experiments performed in the presence of Latrunculin B indicate that the binding between EFA6A and ACTN1 is independent of F-actin. However, F-actin is found around the mitochondria together with EFA6ACter–ActA and ACTN1 suggesting that the EFA6A and ACTN1 couple could organize actin filament structures or even contribute to their nucleation, as proposed for ACTN4 at the AJ (Tang and Brieher, 2012). ARNO was also found to bind directly to ACTN1, through its C-terminal extremity, to modulate neurite extension, suggesting that ACTNs could be a general player in the Arf-regulated actin cytoskeleton (Torii et al., 2012).

Since EFA6A recruits ACTN1, we hypothesized that ACTN1 was acting as its effector. In the past, studying monolayers of MDCK cells, we had found that overexpression of EFA6A accelerates the general program of epithelial polarization, including the assembly of functional TJs (Klein et al., 2008; Luton et al., 2004). Part of the contribution of EFA6A has been attributed to its ability to stabilize the PAMR. Here, by using a 3D cell culture system together with siRNA-mediated depletion, we show that EFA6A is necessary for normal luminogenesis in MDCK cells. Conversely, overexpression of EFA6A increased the proportion of cysts with a SCL and stimulated their enlargement. Thus, we asked whether ACTN1 was acting as an effector to transduce some of the effects of EFA6A on luminogenesis. Indeed, we observed that depletion of ACTN1 blocked the stimulatory effect of EFA6A on both the formation and enlargement of the round SCL. In further support of this idea, depletion of ACTN1 had no additional disruptive impact on cells knocked down for EFA6A. This addition, expression of a mutant of EFA6A deleted of its C-terminus, which contains the ACTN1-binding site, impaired normal luminogenesis. These results demonstrate that ACTN1 is a crucial effector of EFA6A whose function is to promote normal luminogenesis.

To understand the roles of ACTN1, we analyzed in detail the defects induced upon its depletion. In the absence of ACTN1, there was an increase in cysts with multiple lumens, mostly as mini-lumens formed between two cells, or cysts with lumens that failed to extend to all cells. We propose that, in the absence of ACTN1, the initial fusion event to form a PAP is facilitated; however, the subsequent coalescence and extension of lumens to all cells of the aggregate is precluded. In addition, the volumetric growth of the lumens is impaired. In the ACTN1 knockdown cells, the mini-lumens appeared to be essentially blocked at the PAP stage and, in larger cysts, the extended lumens and SCL adopted an octopus-like shape rather than a nice round hollow. Interestingly, in both MDCK and MCF7 cells, in the absence of ACTN1, EFA6 overexpression is capable of rescuing enlargement of the mini-lumens. However, at later stages EFA6A overexpression cannot rescue the enlargement because ACTN1 is required as an effector downstream of EFA6. This implies that the enlargement of the luminal space relies on different molecular machinery at different stages along the process of lumen formation. Thus, ACTN1 is dispensable at the initial stage to create the nascent lumens, but it is essential downstream of EFA6A at later stages for the coalescence, extension and enlargement of the lumens.

ACTN1 is an actin-bundling protein known to regulate the contractility and stiffness of acto-myosin. It competes with myosin-II to bind F-actin in order to maintain a complementary periodicity, which results in linear F-actin bundles with contractile properties. The ratio and distribution of these two proteins determines the overall contractility and rigidity of F-actin cytoskeletons, including that of the PARM (Arnold et al., 2017; Ferrari et al., 2008; Sluysmans et al., 2017). Thus, ACTN1 could act by regulating tension forces at the surface of the developing lumen. Several observations support of this hypothesis. First, EFA6A and ACTN1 depletion reduced the amount of apical pMLC, whereas EFA6A expression stimulated its accumulation at the apical pole in an ACTN1-dependent manner. Second, upon ACTN1 depletion in both MDCK and MCF7 cells, we observed two defects: (1) a stimulatory effect on the initial formation of lumens as indicated by the rapid accumulation of multiple mini-lumens and, (2) at later stages, a defect of maturation (coalescence and extension) that leads to large cysts with several lumens or incomplete lumens. These results are consistent with a role for ACTN1 on contractility or stiffness. Indeed, several independent studies have shown that

decreasing contractility through treatment with blebbistatin, ROCK inhibitors, or downregulation of LKB1 (also known as STK11), an upstream regulator of RhoA, stimulates the initial formation of a lumen at the two-cell stage (Cohen et al., 2007a; Ferrari et al., 2008; Rodríguez-Fraticelli et al., 2012; Taniguchi et al., 2015). Less appreciated is the impact of contractility at later stages. We found that similar to what is seen upon ACTN1 depletion, blebbistatin leads to large cysts with multiple lumens (our unpublished results). A similar observation was made by reducing contractility through depletion of LKB1, which first stimulates the initial formation of lumens but then prevents their coalescence into a SCL (Rodríguez-Fraticelli et al., 2012). Third, supplemental evidence for the role of ACTN1 on contractility came from its effects in RhoAV14-expressing cells. The small G protein RhoA, through its action on the apical PAMR, is a general regulator of the assembly and maintenance of the AJ (Lecuit and Yap, 2015) and TJ (Terry et al., 2010). We showed that ACTN1-depletion could counterbalance the RhoAV14-mediated contractility. We also found that ACTN1-depletion rescued the initial formation of lumens inhibited by RhoAV14 expression. Taken together, these results indicate that luminogenesis is regulated by acto-myosin contractility and stiffness, which should be kept low for the initial formation of a mini-lumen, and then be increased to allow for their coalescence and extension to form a SCL in larger multicellular aggregates.

The implementation of tension forces relies on molecular pickets, which are usually transmembrane proteins that anchor the acto-myosin structures. In polarized epithelial cells, the AJ and TJ are anchor points for the PAMR. It is noteworthy that neither EFA6A nor ACTN1 appeared to be essential for the assembly and positioning of the AJ and TJ, nor the establishment and maintenance of the asymmetry along the apico-basal axis. Thus, EFA6A and its effector ACTN1 modulate the contractility by affecting the activity and/or organization of the apical acto-myosin cytoskeleton and not the anchoring junctional complexes.

Not all the functions of ACTN1 appeared to be mediated through regulating contractility. ACTN1 depletion prevented the luminal enlargement, while the inhibition of contractility by inhibiting myosin-II or LKB1 depletion (Rodríguez-Fraticelli et al., 2012) did not affect the luminal enlargement. Enlargement has been proposed to depend on apical membrane transport involving the delivery of highly charged molecules, hydrostatic pressure mediated by ion channels and coalescence of multilumens. In ACTN1-depleted cells, the surface of the apical membrane appears large enough to accommodate a bigger luminal volume. In addition, the highly charged PDX protein is properly delivered and coalescence is not relevant when considering SCLs with an octopus-like shape. However, ACTN1 could help to retain polycystins, which are implicated in intercellular mechanotransduction (Li et al., 2005); Wilson, 2001), as well as ion channels. In fact, many ion channels have been shown to bind or to require ACTNs in order for them to be retained at the cell surface (Cukovic et al., 2001; Lu et al., 2009; Maruoka et al., 2000; Sadeghi et al., 2002; Schnizler et al., 2009; Wyszynski et al., 1997; Ziane et al., 2010). EFA6A was also shown to bind the ion channels TWIK1 and Kir3.4 (Decressac et al., 2004; Gong et al., 2007). Furthermore, it has been reported that ACTN4 regulates the outwards water transport in a process called regulatory volume decrease in response to osmotic swelling (Ando-Akatsuka et al., 2012). In summary, together with EFA6A, the recruitment of ACTN1 to the apical surface might help stabilize ion channels regulating fluid influx and consequently lumen enlargement.

Alternatively, ACTN1 could serve to organize a non-contractile scaffold to help support the spherical architecture of the luminal membrane. To do so, ACTN1 could participate by bundling F-actin filaments into rigid structures and/or could serve to link or even nucleate actin filaments at the AJ or TJ to anchor the luminal actin cytoskeleton. Such a role has been proposed for ACTN4 at the level of the AJ (Tang and Brieher, 2012).

Finally, we examined the role of ACTN1 in the human tumoral mammary cell line MCF7. When grown in 3D culture, these cells fail to assemble TJ, form a lumen or polarize (Han et al., 2010; Kenny et al., 2007; Zangari et al., 2014). Only a small fraction of cell aggregates display one or several mini-lumens. As shown in the past, EFA6B expression stimulated the formation of extended lumens and restored an epithelial-like phenotype. So, in contrast to MDCK cells, the formation of extended lumens in MCF7 is strictly dependent on the expression of VSV-G–EFA6B. Thus, these cells make a good model to study the role of ACTN1 downstream of EFA6B. Indeed, ACTN1 depletion totally blocked lumen formation, demonstrating that ACTN1 is a crucial effector for EFA6B in the induction of luminogenesis. Furthermore, ACTN1-depletion in wild-type MCF7 cells stimulated the formation of multiple mini-lumens that were blocked at the PAP stage. EFA6B expression did not rescue the formation of extended lumens but did enlarge their volume. Thus, in agreement with our observations in MDCK cells, ACTN1 depletion favors the initial formation of lumens in between two cells but prevents their coalescence and enlargement.

In conclusion, we show that ACTN1 is an effector of EFA6A and EFA6B to promote luminogenesis in normal and tumoral cell models. We propose a scenario whereby, at the onset of luminogenesis, the acto-myosin contractility and rigidity must be kept low to relax the sub-membranous actin cytoskeleton where vesicle fusion occurs at the AMIS. At this stage, EFA6 proteins have a stimulatory effect on the formation and the enlargement of the mini-lumens suggesting that it acts through an effector other than ACTN1; perhaps through Arf6, which has already been shown to be involved in luminogensis (Tushir et al., 2010; Zangari et al., 2014). At a later stage, EFA6 proteins recruit ACTN1 to contribute to the coalescence of the mini-lumens, their extension to neighboring cells and enlargement. We do not exclude the possibility that EFA6 proteins could recruit other effectors to mediate its effects. Nevertheless, ACTN1 is certainly a primary effector that might act by modulating the contractility of the acto-myosin ring and thereby mediating its effects on coalescence and extension (by helping to pull the lumens together and breaking through the junctional complexes). Given these results, the EFA6A–ACTN1 pathway might be important for tubulogenesis occurring through the cord hollowing mechanism, where multiple mini-lumens are formed along the tubular structure and subsequently fuse to coalesce in a single lumen, in a ROCK–myosin II-dependent manner (Bernascone et al., 2017; Kim et al., 2015; Sigurbjörnsdóttir et al., 2014).

In summary, we identified and characterized the role of two new regulators of luminogenesis: EFA6A and ACTN1. ACTN1 behaves as an effector to transduce the stimulating effect of EFA6A on the formation of a single and well-expanded central lumen by facilitating the extension and enlargement stages. The EFA6A–ACTN1 couple acts, at least in part, by balancing the contractility of the cortical acto-myosin cytoskeleton. In the tumoral MCF7 cells, this pathway has the capacity to restore the apico-basal polarization, TJ assembly and collective cellular organization into a cyst with a central lumen pointing to new directions for cancer research and therapy.

Journal of Cell Science (2018) 131, jcs209361. doi:10.1242/jcs.209361

MATERIALS AND METHODS

Cells, media and transfection

BHK cells were grown in Glasgow's minimum essential medium (GMEM; Invitrogen, Paris, France) supplemented with 5% heat decomplemented fetal calf serum (FCS; Biowest-Abcys, Nuaillé, France) and penicillin-streptomycin (Invitrogen). Transient transfection was performed by lipofection using JETPEI (Polyplus Transfection, Illkirck, France). MDCK clone II cells expressing VSV-G–EFA6A, VSV-G–EFA6AΔC (Luton et al., 2004) or Myc-RhoAV14 (Jou and Nelson, 1998) under the control of the tetracycline-repressible transactivator were grown in MEM (Sigma-Aldrich, Saint-Quentin-Fallavier, France), 5% decomplemented FCS (Biowest-Abcys), penicillin-streptomycin and 20 ng/ml doxycycline. Expression of EFA6A and RhoAV14 was induced upon removal of doxycycline. Plasmids and siRNA transfections were performed by nucleofection (Nucleofector™; Lonza, Köln, Germany). For stable expression of ACTN1–GFP, ACTN4–GFP and ACTN1S744–GFP, the cells were selected with geneticin (Invitrogen) 2 days after transfection. MCF7 and MCF7-VSV-G–EFA6B (Zangari et al., 2014) were grown in Dulbecco's modified Eagle's medium (DMEM; Sigma-Aldrich) containing 10% decomplemented FCS (Hyclone™, GE Healthcare, France), supplemented with insulin, transferrin, selenium, glutamine, sodium pyruvate, MEM non-essential amino-acids and penicillin-streptomycin (all from Invitrogen). Transient transfection was performed by nucleofection. For 3D cell culture, 10^4 cells were mixed with 20 µl of 5 mg/ml Matrigel (BD Biosciences, Le Pont de Claix, France) deposited as a drop on a 12 mm glass coverslip. The BHK and MCF7 cells were obtained from the ATCC and authenticated by short tandem repeat profiling by the vendor. The parental MDCK II cell line was from Dr Keith Mostov (University of California, San Francisco, USA). MDCK and derived cell lines were tested for species specificity. Newly thawed cells from frozen stocks were tested for absence of mycoplasma contamination and used for 10 passages before replacement.

Antibodies and reagents

Rabbit polyclonal sera specific for EFA6B (HPA034722; Sigma-Aldrich), occludin (71-1500, Invitrogen), phosphorylated (Thr18/Ser19) myosin light chain 2 (3674, Cell Signaling Technology, Leiden, The Netherlands), the PI3K p85 regulatory subunit (ABS234, Millipore, Molsheim, France), Hsp60 (Ab46798, Abcam, Paris, France), GST (27-4577-01, GE Healthcare) were used. Mouse monoclonal antibodies specific for gp135/podocalyxin (3B8; gift from George Ojakian, State University of New York Downstate Medical Center), the VSV-G tag (P5D4; Roche Diagnostics, Mannheim, Germany), actin (AC-40; Sigma-Aldrich), E-cadherin (36; Invitrogen), paxillin (610052, BD Biosciences), the 6× histidine tag (HIS1; Sigma-Aldrich), the Myc tag (9E10 and rat hybridoma 3F10; Roche Diagnostics), GFP (7.1, Roche Diagnostics), ACTN1 (BM75.2; Sigma-Aldrich and H-2; Santa Cruz Biotechnology, Heidelberg, Germany) were used. The rabbit polyclonal anti-EFA6A was as described elsewhere (Sakagami et al., 2007). The horseradish peroxidase (HRP)-coupled and fluorescent probes (secondary antibodies, phalloidin and DAPI) were from Jackson ImmunoResearch Labs (Suffolk, UK) and Molecular Probes (Eugene, Oregon, USA), respectively. Full details of antibodies, including dilutions used are given in Table S1. All other reagents and chemicals were from Sigma-Aldrich.

DNA constructs and siRNA

Constructs for the expression of the following proteins have been described elsewhere: GFP–EFA6A (Decressac et al., 2004), mRFP–EFA6A (Théard et al., 2010), GST–EFA6A, GST–EFA6ACter (Macia et al., 2008), (6xhis)–EFA6A (Macia et al., 2008), βarrestin1Cter–GFP (Scott et al., 2002), the GST–ABD [amino acids (aa) 1–269], GST–SRD (aa 218–749) and GST–CAMD (aa 713–887) fragments of ACTN1 (Fraley et al., 2003), ACTN1–GFP (Rajfur et al., 2002), GST–ACTN4 (Khurana et al., 2011), ACTN4–HA and ACTN4–GFP (Michaud et al., 2006). The GST–ACTN1 construct was prepared by PCR amplification of full-length ACTN1 from pEGFP-ACTN1 and cloned into EcoR1 and Xho1 sites of the pGEX4T1 using the following primers:5′-GATCGATCGAATTCATGGACCATTATGATTCTCAG-3′ and 5′-TGTATCACTCGAGTTAGAGGTCACTCTCGCCGTAC-3′. The siRNA #2225 insensitive ACTN1–GFP was generated by introducing silent mutations at positions 2236, 2237 and 2238 (aa Ser744) using the QuikChange mutagenesis kit (Agilent Technologies, Courtabœuf, France) using the following primers 5′-GCCAAGGGCATCTCGCAGGAGCAGATGAATG-3′ and 5′-CATTCATCTGCTCCTGCGAGATGCCCTTGGC-3′. The resulting plasmid was termed ACTN1S744–GFP. Full-length EFA6A and EFA6ACter were cloned into mRFP-N1-ActA (Benjamin et al., 2010) by PCR amplification at the EcoRI and SacII sites. Primers used to amplify and clone the full-length EFA6A were 5′-GATCGATCGAATTCGCCGCCACCATGCCTCTCAAGTCACCTGTG-3′ and 5′-GATCGATCCCGCGGGGGCTTCCGCCGCCCACTGCC-3′, and those for the EFA6ACter fragment were 5′-GATCGATCGAATTCGCCGCCACCATGTTCTCTGCGCCCCCCTTCC-3′ and 5′-GATCGATCCCGCGGGGGCTTCCGCCGCCCACTGCC-3′. The resulting plasmids were termed EFA6A–mRFP–ActA and EFA6ACter–mRFP–ActA.

The specific and control siRNAs were designed and obtained from Eurogentec (Angers, France) and Sigma-Aldrich. The silencing efficiency of several siRNAs per target was assessed by immunoblotting (Figs S3 and S4). Knockdown of canine EFA6A and ACTN1 expression in MDCK cells was carried out using the siRNA #2661 5′-CCUAUCAGAGGCGGAGCUA-3′ or #1440 5′-CUCUUUCAGUUGUGUGUUU-3′ and siRNA #2225 5′-GCAUCAGCCAGGAGCAAAU-3′ or #594 5′-GGACGACCCACUCACAAAU-3′, respectively. Knockdown of human ACTN1 expression in MCF7 cells was carried out using the siRNA #1789 5′-CCUCAGGAGAUCAAUGGCAAA-3′. Silencing specificity was verified with control siRNAs, rescue experiments (Fig. 3C and Fig. 4B) and additional independent siRNA (Fig. S4).

Recombinant proteins, pull-down assay and immunoprecipitation

The induction and purification of GST constructs with glutathione–sepharose CL-4B beads (GE Healthcare) was as previously described (Macia et al., 2008). The N-terminal 6×his–EFA6A was purified on Ni-NTA columns according to the manufacturer's instructions (Qiagen, Courtabœuf, France). For the GST-EFA6A pull-down from cell lysates, MDCK-ACTN1–GFP cells were lysed at 4°C in 0.5% Nonidet P-40, 20 mM Hepes pH 7.4, 125 mM NaCl, 1 mM phenylmethylsulphonyl fluoride (PMSF) and a cocktail of protease inhibitors (Complete™, Roche Diagnostics). The cleared lysates were incubated for 4 h at 4°C with 1.5 µM of the indicated GST-fused proteins and 30 µl of glutathione-sepharose CL-4B beads. After three washes in lysis buffer, the beads were boiled in Laemmli buffer, submitted to SDS-PAGE and the proteins revealed by immunoblotting. For the GST pull-down of purified His–EFA6A, 10 µM of the indicated GST fusion proteins and 10 µM of His–EFA6A were incubated together for 2 h at 4°C, and the experiments carried on as described above. For all GST pulldown experiments, an aliquot of the mixture was analyzed by SDS-PAGE followed by immunoblotting to estimate the total amount of the added proteins. For immunoprecipitation, cells were solubilized in ice-cold Triton X-100 lysis buffer (1% Triton X-100, 150 mM NaCl, 5 mM EDTA, 20 mM Triethanolamine-HCl pH 8.1 and 1 mM PMSF). After centrifugation for 20 min at 16,000 ***g*** at 4°C, the supernatants were pre-cleared at 4°C for 10 min, centrifuged for 10 min at 16,000 ***g*** and combined with protein A–sepharose and the indicated antibody overnight at 4°C. The beads were then washed three times in washing buffer (1% Triton X-100, 0.2% SDS, 150 mM NaCl, 5 mM EDTA, 8% sucrose, 1 mM PMSF and the cocktail of protease inhibitors) and washed once in washing buffer without detergent. The immunoprecipitates were then resuspended and boiled for 5 min in Laemmli buffer before SDS-PAGE and immunoblot analysis.

Immunoblotting

Samples were resolved on SDS-PAGE and proteins transferred onto a nitrocellulose membrane. Membrane blocking (30 min at room temperature) and antibody dilutions were performed in PBS with 5% non-fat dried milk. The membranes were incubated overnight at 4°C with the indicated antibody. The proteins were revealed by chemiluminescence (ECL, Amersham, GE Healthcare) using secondary antibodies directly coupled

to HRP. The membranes were analyzed with the luminescent image analyzer LAS-3000 (Fujifilm, Saint-Quentin-en-Yvelines, France).

Immunofluorescence

Cells were fixed in 4% PFA, the samples processed as previously described (Luton et al., 2004) and imaged on a confocal microscope (Leica TCS-SP5, Nanterre, France and Zeiss LSM780, Marly-le-Roi, France). Images were processed for presentation using NIH Image and Adobe® Photoshop® CS2 software.

Quantification of luminogenesis

Unless specified, all quantifications were from cysts of 4–15 cells obtained after 48 to 72 h growth in Matrigel. Experiments were repeated at least three times in triplicate and a minimum of 100 cysts per experimental replicate were analyzed. Each cell aggregate was scanned by using confocal microscopy to analyze the shape of the lumens and determine the presence of a single lumen or multiple lumens. Cysts were classified within five categories: cysts with a single central opened lumen (SCL), two or more lumens regardless of their shape (multilumen), with an opened lumen but that was not extended to all cells (incomplete lumen), with an optically closed lumen (otherwise named pre-apical patch, PAP), and with no lumen. Within the SCL class, we discriminated those lumens that were well enlarged from those that were barely opened and not expanded displaying an 'octopus-like' shape (see Fig. 3B). Note, that cysts with dividing cells or with lumen-containing cells and/or nuclei were not included. In addition, a separate quantification was performed for a lumen opened only in between two cells (mini-lumen) as they fell in the multilumen, incomplete and optically closed lumen categories (see Fig. 3E). Enlargement refers to the increase of the luminal volume. When enlargement was compromised there was an octopus-like lumen. Extension refers to the opening of a lumen (in general starting in-between two cells) to all the cells of the cell aggregate or coalescence of multiple small lumens to eventually form a single lumen. When extension was compromised it led to an incomplete lumen and/or to the presence of multiple lumens including mini-lumens (see Fig. 3D,E).

Statistics

The experiments were performed at least three times in triplicate, and data from all experiments were combined. Values are mean±s.d. Statistical significance was calculated with a two-tailed Student's *t*-test. Non-significant difference (N.S.) are $P>0.05$; *$P\leq0.05$; **$P\leq0.01$; ***$P\leq0.001$.

Acknowledgements

We thank Drs Hiroyuki Sakagami (Kitasato University, Japan) for the EFA6A-specific anti-serum, James Nelson (Stanford University, USA) for the MDCK-RhoAV14 cells and the ActA–mRFP plasmid, Dr Jeffery Greenwood (Oregon State University, USA) for the plasmids encoding the three fragments of GST–ACTN1 and GFP–ACTN1, Dr Chris Kennedy (University of Ottawa, Canada) for plasmids encoding HA–ACTN4 and GFP–ACTN4, and Dr Hung-Ying Kao (Case Western Reserve University, USA) for plasmid encoding GST–ACTN4. We are grateful to K. L. Singer for critical reading of the manuscript.

Competing interests

The authors declare no competing or financial interests.

Author contributions

Conceptualization: J.M., F.L.; Methodology: J.M., R.F., M.P., P.L., F.L.; Validation: J.M., M.P., P.L., F.L.; Formal analysis: J.M., R.F., M.P., P.L., J.-P.B., M.F., F.L.; Investigation: J.M., F.L.; Data curation: J.M., F.L.; Writing - original draft: J.M., F.L.; Writing - review & editing: J.M., R.F., M.F.; Visualization: M.F., F.L.; Supervision: J.-P.B., M.F., F.L.; Project administration: F.L.; Funding acquisition: J.-P.B., M.F., F.L.

Funding

This work was supported by Fondation ARC pour la Recherche sur le Cancer, and Agence Nationale de la Recherche (ANR) through the 'Investments for the Future' LABEX SIGNALIFE (program reference ANR-11-LABX-0028-01). R.F. was the recipient of a PhD fellowship from the Labex SIGNALIFE program. J.-P.B. is funded by La Ligue Contre le Cancer, Cancéropôle PACA and SIRIC (INCa-DGOS-Inserm 6038). J.-P.B. is a scholar of Institut Universitaire de France.

Supplementary information

Supplementary information available online at
http://jcs.biologists.org/lookup/doi/10.1242/jcs.209361.supplemental

References

Altschuler, Y., Liu, S.-H., Katz, L., Tang, K., Hardy, S., Brodsky, F., Apodaca, G. and Mostov, K. (1999). ADP-ribosylation factor 6 and endocytosis at the apical surface of Madin-Darby canine kidney cells. *J. Cell Biol.* **147**, 7-12.

Ando-Akatsuka, Y., Shimizu, T., Numata, T. and Okada, Y. (2012). Involvements of the ABC protein ABCF2 and alpha-actinin-4 in regulation of cell volume and anion channels in human epithelial cells. *J. Cell. Physiol.* **227**, 3498-3510.

Arnold, T. R., Stephenson, R. E. and Miller, A. L. (2017). Rho GTPases and actomyosin: partners in regulating epithelial cell-cell junction structure and function. *Exp. Cell Res.* **358**, 20-30.

Benjamin, J. M., Kwiatkowski, A. V., Yang, C., Korobova, F., Pokutta, S., Svitkina, T., Weis, W. I. and Nelson, W. J. (2010). AlphaE-catenin regulates actin dynamics independently of cadherin-mediated cell-cell adhesion. *J. Cell Biol.* **189**, 339-352.

Bernascone, I., Hachimi, M. and Martin-Belmonte, F. (2017). Signaling networks in epithelial tube formation. *Cold Spring Harb. Perspect. Biol.* **9**, pii: a027946.

Blasky, A. J., Mangan, A. and Prekeris, R. (2015). Polarized protein transport and lumen formation during epithelial tissue morphogenesis. *Annu. Rev. Cell Dev. Biol.* **31**, 575-591.

Braga, V. (2016). Spatial integration of E-cadherin adhesion, signalling and the epithelial cytoskeleton. *Curr. Opin. Cell Biol.* **42**, 138-145.

Bubeck, P., Pistor, S., Wehland, J. and Jockusch, B. M. (1997). Ligand recruitment by vinculin domains in transfected cells. *J. Cell Sci.* **110**, 1361-1371.

Burridge, K. and Wittchen, E. S. (2013). The tension mounts: stress fibers as force-generating mechanotransducers. *J. Cell Biol.* **200**, 9-19.

Chen, V. C., Li, X., Perreault, H. and Nagy, J. I. (2006). Interaction of zonula occludens-1 (ZO-1) with alpha-actinin-4: application of functional proteomics for identification of PDZ domain-associated proteins. *J. Proteome Res.* **5**, 2123-2134.

Cohen, D., Tian, Y. and Musch, A. (2007a). Par1b promotes hepatic-type lumen polarity in Madin Darby canine kidney cells via myosin II- and E-cadherin-dependent signaling. *Mol. Biol. Cell* **18**, 2203-2215.

Cohen, L. A., Honda, A., Varnai, P., Brown, F. D., Balla, T. and Donaldson, J. G. (2007b). Active Arf6 recruits ARNO/cytohesin GEFs to the PM by binding their PH domains. *Mol. Biol. Cell* **18**, 2244-2253.

Coravos, J. S. and Martin, A. C. (2016). Apical sarcomere-like actomyosin contracts nonmuscle Drosophila epithelial cells. *Dev. Cell* **39**, 346-358.

Coravos, J. S., Mason, F. M. and Martin, A. C. (2017). Actomyosin pulsing in tissue integrity maintenance during morphogenesis. *Trends Cell Biol.* **27**, 276-283.

Cukovic, D., Lu, G. W.-K., Wible, B., Steele, D. F. and Fedida, D. (2001). A discrete amino terminal domain of Kv1.5 and Kv1.4 potassium channels interacts with the spectrin repeats of alpha-actinin-2. *FEBS Lett.* **498**, 87-92.

D'Souza-Schorey, C. and Chavrier, P. (2006). ARF proteins: roles in membrane traffic and beyond. *Nat. Rev. Mol. Cell Biol.* **7**, 347-358.

Datta, A., Bryant, D. M. and Mostov, K. E. (2011). Molecular regulation of lumen morphogenesis. *Curr. Biol.* **21**, R126-R136.

Decressac, S., Franco, M., Bendahhou, S., Warth, R., Knauer, S., Barhanin, J., Lazdunski, M. and Lesage, F. (2004). ARF6-dependent interaction of the TWIK1 K+ channel with EFA6, a GDP/GTP exchange factor for ARF6. *EMBO Rep.* **5**, 1171-1175.

Derrien, V., Couillault, C., Franco, M., Martineau, S., Montcourrier, P., Houlgatte, R. and Chavrier, P. (2002). A conserved C-terminal domain of EFA6-family ARF6-guanine nucleotide exchange factors induces lengthening of microvilli-like membrane protrusions. *J. Cell Sci.* **115**, 2867-2879.

DiNitto, J. P., Delprato, A., Gabe Lee, M.-T., Cronin, T. C., Huang, S., Guilherme, A., Czech, M. P. and Lambright, D. G. (2007). Structural basis and mechanism of autoregulation in 3-phosphoinositide-dependent Grp1 family Arf GTPase exchange factors. *Mol. Cell* **28**, 569-583.

DuFort, C. C., Paszek, M. J. and Weaver, V. M. (2011). Balancing forces: architectural control of mechanotransduction. *Nat. Rev. Mol. Cell Biol.* **12**, 308-319.

Ebrahim, S., Fujita, T., Millis, B. A., Kozin, E., Ma, X., Kawamoto, S., Baird, M. A., Davidson, M., Yonemura, S., Hisa, Y. et al. (2013). NMII forms a contractile transcellular sarcomeric network to regulate apical cell junctions and tissue geometry. *Curr. Biol.* **23**, 731-736.

Ferrari, A., Veligodskiy, A., Berge, U., Lucas, M. S. and Kroschewski, R. (2008). ROCK-mediated contractility, tight junctions and channels contribute to the conversion of a preapical patch into apical surface during isochoric lumen initiation. *J. Cell Sci.* **121**, 3649-3663.

Foley, K. S. and Young, P. W. (2013). An analysis of splicing, actin-binding properties, heterodimerization and molecular interactions of the non-muscle alpha-actinins. *Biochem. J.* **452**, 477-488.

Foley, K. S. and Young, P. W. (2014). The non-muscle functions of actinins: an update. *Biochem. J.* **459**, 1-13.

Franco, M., Peters, P. J., Boretto, J., van Donselaar, E., Neri, A., D'Souza-Schorey, C. and Chavrier, P. (1999). EFA6, a sec7 domain-containing exchange

factor for ARF6, coordinates membrane recycling and actin cytoskeleton organization. *EMBO J.* **18**, 1480-1491.
Fraley, T. S., Tran, T. C., Corgan, A. M., Nash, C. A., Hao, J., Critchley, D. R. and Greenwood, J. A. (2003). Phosphoinositide binding inhibits alpha-actinin bundling activity. *J. Biol. Chem.* **278**, 24039-24045.
Geiger, B., Tokuyasu, K. T. and Singer, S. J. (1979). Immunocytochemical localization of alpha-actinin in intestinal epithelial cells. *Proc. Natl. Acad. Sci. USA* **76**, 2833-2837.
Gillingham, A. K. and Munro, S. (2007). The small G proteins of the Arf family and their regulators. *Annu. Rev. Cell Dev. Biol.* **23**, 579-611.
Gong, Q., Weide, M., Huntsman, C., Xu, Z., Jan, L. Y. and Ma, D. (2007). Identification and characterization of a new class of trafficking motifs for controlling clathrin-independent internalization and recycling. *J. Biol. Chem.* **282**, 13087-13097.
Grikscheit, K. and Grosse, R. (2016). Formins at the Junction. *Trends Biochem. Sci.* **41**, 148-159.
Han, J., Chang, H., Giricz, O., Lee, G. Y., Baehner, F. L., Gray, J. W., Bissell, M. J., Kenny, P. A. and Parvin, B. (2010). Molecular predictors of 3D morphogenesis by breast cancer cell lines in 3D culture. *PLoS Comput. Biol.* **6**, e1000684.
Honda, K., Yamada, T., Endo, R., Ino, Y., Gotoh, M., Tsuda, H., Yamada, Y., Chiba, H. and Hirohashi, S. (1998). Actinin-4, a novel actin-bundling protein associated with cell motility and cancer invasion. *J. Cell Biol.* **140**, 1383-1393.
Iskratsch, T., Wolfenson, H. and Sheetz, M. P. (2014). Appreciating force and shape – the rise of mechanotransduction in cell biology. *Nat. Rev. Mol. Cell Biol.* **15**, 825-833.
Jahed, Z., Shams, H., Mehrbod, M. and Mofrad, M. R. K. (2014). Mechanotransduction pathways linking the extracellular matrix to the nucleus. *Int. Rev. Cell Mol. Biol.* **310**, 171-220.
Jaworski, J. (2007). ARF6 in the nervous system. *Eur. J. Cell Biol.* **86**, 513-524.
Jou, T.-S. and Nelson, W. J. (1998). Effects of regulated expression of mutant RhoA and Rac1 small GTPases on the development of epithelial (MDCK) cell polarity. *J. Cell Biol.* **142**, 85-100.
Kenny, P. A., Lee, G. Y., Myers, C. A., Neve, R. M., Semeiks, J. R., Spellman, P. T., Lorenz, K., Lee, E. H., Barcellos-Hoff, M. H., Petersen, O. W. et al. (2007). The morphologies of breast cancer cell lines in three-dimensional assays correlate with their profiles of gene expression. *Mol. Oncol.* **1**, 84-96.
Khurana, S., Chakraborty, S., Cheng, X., Su, Y. T. and Kao, H. Y. (2011). The actin-binding protein, actinin alpha 4 (ACTN4), is a nuclear receptor coactivator that promotes proliferation of MCF-7 breast cancer cells. *J. Biol. Chem.* **286**, 1850-1859.
Kim, M., Shewan, A. M., Ewald, A. J., Werb, Z. and Mostov, K. E. (2015). p114RhoGEF governs cell motility and lumen formation during tubulogenesis through a ROCK-myosin-II pathway. *J. Cell Sci.* **128**, 4317-4327.
Klein, S., Partisani, M., Franco, M. and Luton, F. (2008). EFA6 facilitates the assembly of the tight junction by coordinating an Arf6-dependent and -independent pathway. *J. Biol. Chem.* **283**, 30129-30138.
Le Clainche, C. and Carlier, M.-F. (2008). Regulation of actin assembly associated with protrusion and adhesion in cell migration. *Physiol. Rev.* **88**, 489-513.
Lecuit, T. and Yap, A. S. (2015). E-cadherin junctions as active mechanical integrators in tissue dynamics. *Nat. Cell Biol.* **17**, 533-539.
Li, Q., Montalbetti, N., Shen, P. Y., Dai, X.-Q., Cheeseman, C. I., Karpinski, E., Wu, G., Cantiello, H. F. and Chen, X.-Z. (2005). Alpha-actinin associates with polycystin-2 and regulates its channel activity. *Hum. Mol. Genet.* **14**, 1587-1603.
Lu, L., Timofeyev, V., Li, N., Rafizadeh, S., Singapuri, A., Harris, T. R. and Chiamvimonvat, N. (2009). Alpha-actinin2 cytoskeletal protein is required for the functional membrane localization of a Ca2+-activated K+ channel (SK2 channel). *Proc. Natl. Acad. Sci. USA* **106**, 18402-18407.
Luton, F., Klein, S., Chauvin, J. P., Le Bivic, A., Bourgoin, S., Franco, M. and Chardin, P. (2004). EFA6, exchange factor for ARF6, regulates the actin cytoskeleton and associated tight junction in response to E-cadherin engagement. *Mol. Biol. Cell* **15**, 1134-1145.
Macia, E., Partisani, M., Favard, C., Mortier, E., Zimmermann, P., Carlier, M.-F., Gounon, P., Luton, F. and Franco, M. (2008). The pleckstrin homology domain of the Arf6-specific exchange factor EFA6 localizes to the plasma membrane by interacting with phosphatidylinositol 4,5-bisphosphate and F-actin. *J. Biol. Chem.* **283**, 19836-19844.
Macia, E., Partisani, M., Paleotti, O., Luton, F. and Franco, M. (2012). Arf6 negatively controls the rapid recycling of the beta2 adrenergic receptor. *J. Cell Sci.* **125**, 4026-4035.
Martin, A. C. and Goldstein, B. (2014). Apical constriction: themes and variations on a cellular mechanism driving morphogenesis. *Development* **141**, 1987-1998.
Martin-Belmonte, F. and Perez-Moreno, M. (2011). Epithelial cell polarity, stem cells and cancer. *Nat. Rev. Cancer* **12**, 23-38.
Maruoka, N. D., Steele, D. F., Au, B. P.-Y., Dan, P., Zhang, X., Moore, E. D. W. and Fedida, D. (2000). alpha-actinin-2 couples to cardiac Kv1.5 channels, regulating current density and channel localization in HEK cells. *FEBS Lett.* **473**, 188-194.
Michaud, J. L., Chaisson, K. M., Parks, R. J. and Kennedy, C. R. (2006). FSGS-associated alpha-actinin-4 (K256E) impairs cytoskeletal dynamics in podocytes. *Kidney Int.* **70**, 1054-1061.
Moeller, M. J., Soofi, A., Braun, G. S., Li, X., Watzl, C., Kriz, W. and Holzman, L. B. (2004). Protocadherin FAT1 binds Ena/VASP proteins and is necessary for actin dynamics and cell polarization. *EMBO J.* **23**, 3769-3779.
Murrell, M., Oakes, P. W., Lenz, M. and Gardel, M. L. (2015). Forcing cells into shape: the mechanics of actomyosin contractility. *Nat. Rev. Mol. Cell Biol.* **16**, 486-498.
Nakatsuji, H., Nishimura, N., Yamamura, R., Kanayama, H. O. and Sasaki, T. (2008). Involvement of actinin-4 in the recruitment of JRAB/MICAL-L2 to cell-cell junctions and the formation of functional tight junctions. *Mol. Cell. Biol.* **28**, 3324-3335.
Oakes, P. W., Beckham, Y., Stricker, J. and Gardel, M. L. (2012). Tension is required but not sufficient for focal adhesion maturation without a stress fiber template. *J. Cell Biol.* **196**, 363-374.
Padovani, D., Folly-Klan, M., Labarde, A., Boulakirba, S., Campanacci, V., Franco, M., Zeghouf, M. and Cherfils, J. (2014). EFA6 controls Arf1 and Arf6 activation through a negative feedback loop. *Proc. Natl. Acad. Sci. USA* **111**, 12378-12383.
Palacios, F., Price, L., Schweitzer, J., Collard, J. G. and D'Souza-Schorey, C. (2001). An essential role for ARF6-regulated membrane traffic in adherens junction turnover and epithelial cell migration. *EMBO J.* **20**, 4973-4986.
Palacios, F., Schweitzer, J. K., Boshans, R. L. and D'Souza-Schorey, C. (2002). ARF6-GTP recruits Nm23-H1 to facilitate dynamin-mediated endocytosis during adherens junctions disassembly. *Nat. Cell Biol.* **4**, 929-936.
Palacios, F., Tushir, J. S., Fujita, Y. and D'Souza-Schorey, C. (2005). Lysosomal targeting of E-cadherin: a unique mechanism for the down-regulation of cell-cell adhesion during epithelial to mesenchymal transitions. *Mol. Cell. Biol.* **25**, 389-402.
Parsons, J. T., Horwitz, A. R. and Schwartz, M. A. (2010). Cell adhesion: integrating cytoskeletal dynamics and cellular tension. *Nat. Rev. Mol. Cell Biol.* **11**, 633-643.
Quiros, M. and Nusrat, A. (2014). RhoGTPases, actomyosin signaling and regulation of the epithelial Apical Junctional Complex. *Semin. Cell Dev. Biol.* **36**, 194-203.
Rajfur, Z., Roy, P., Otey, C., Romer, L. and Jacobson, K. (2002). Dissecting the link between stress fibres and focal adhesions by CALI with EGFP fusion proteins. *Nat. Cell Biol.* **4**, 286-293.
Reinhard, M., Zumbrunn, J., Jaquemar, D., Kuhn, M., Walter, U. and Trueb, B. (1999). An alpha-actinin binding site of zyxin is essential for subcellular zyxin localization and alpha-actinin recruitment. *J. Biol. Chem.* **274**, 13410-13418.
Rodríguez-Fraticelli, A. E., Auzan, M., Alonso, M. A., Bornens, M. and Martín-Belmonte, F. (2012). Cell confinement controls centrosome positioning and lumen initiation during epithelial morphogenesis. *J. Cell Biol.* **198**, 1011-1023.
Röper, K. (2015). Integration of cell-cell adhesion and contractile actomyosin activity during morphogenesis. *Curr. Top. Dev. Biol.* **112**, 103-127.
Sabe, H., Hashimoto, S., Morishige, M., Ogawa, E., Hashimoto, A., Nam, J.-M., Miura, K., Yano, H. and Onodera, Y. (2009). The EGFR-GEP100-Arf6-AMAP1 signaling pathway specific to breast cancer invasion and metastasis. *Traffic* **10**, 982-993.
Sadeghi, A., Doyle, A. D. and Johnson, B. D. (2002). Regulation of the cardiac L-type Ca2+ channel by the actin-binding proteins alpha-actinin and dystrophin. *Am. J. Physiol. Cell Physiol.* **282**, C1502-C1511.
Sakagami, H. (2008). The EFA6 family: guanine nucleotide exchange factors for ADP ribosylation factor 6 at neuronal synapses. *Tohoku J. Exp. Med.* **214**, 191-198.
Sakagami, H., Honma, T., Sukegawa, J., Owada, Y., Yanagisawa, T. and Kondo, H. (2007). Somatodendritic localization of EFA6A, a guanine nucleotide exchange factor for ADP-ribosylation factor 6, and its possible interaction with alpha-actinin in dendritic spines. *Eur. J. Neurosci.* **25**, 618-628.
Schnizler, M. K., Schnizler, K., Zha, X. M., Hall, D. D., Wemmie, J. A., Hell, J. W. and Welsh, M. J. (2009). The cytoskeletal protein alpha-actinin regulates acid-sensing ion channel 1a through a C-terminal interaction. *J. Biol. Chem.* **284**, 2697-2705.
Schweitzer, J. K., Sedgwick, A. E. and D'Souza-Schorey, C. (2011). ARF6-mediated endocytic recycling impacts cell movement, cell division and lipid homeostasis. *Semin. Cell Dev. Biol.* **22**, 39-47.
Scott, M. G., Benmerah, A., Muntaner, O. and Marullo, S. (2002). Recruitment of activated G protein-coupled receptors to pre-existing clathrin-coated pits in living cells. *J. Biol. Chem.* **277**, 3552-3559.
Sigurbjörnsdóttir, S., Mathew, R. and Leptin, M. (2014). Molecular mechanisms of de novo lumen formation. *Nat. Rev. Mol. Cell Biol.* **15**, 665-676.
Sironi, C., Teesalu, T., Muggia, A., Fontana, G., Marino, F., Savaresi, S. and Talarico, D. (2009). EFA6A encodes two isoforms with distinct biological activities in neuronal cells. *J. Cell Sci.* **122**, 2108-2118.
Sluysmans, S., Vasileva, E., Spadaro, D., Shah, J., Rouaud, F. and Citi, S. (2017). The role of apical cell-cell junctions and associated cytoskeleton in mechanotransduction. *Biol. Cell* **109**, 139-161.
Stalder, D., Barelli, H., Gautier, R., Macia, E., Jackson, C. L. and Antonny, B. (2011). Kinetic studies of the Arf activator Arno on model membranes in the presence of Arf effectors suggest control by a positive feedback loop. *J. Biol. Chem.* **286**, 3873-3883.

Stossel, T. P., Condeelis, J., Cooley, L., Hartwig, J. H., Noegel, A., Schleicher, M. and Shapiro, S. S. (2001). Filamins as integrators of cell mechanics and signalling. *Nat. Rev. Mol. Cell Biol.* **2**, 138-145.

Takeichi, M. (2014). Dynamic contacts: rearranging adherens junctions to drive epithelial remodelling. *Nat. Rev. Mol. Cell Biol.* **15**, 397-410.

Tang, V. W. and Brieher, W. M. (2012). alpha-Actinin-4/FSGS1 is required for Arp2/3-dependent actin assembly at the adherens junction. *J. Cell Biol.* **196**, 115-130.

Taniguchi, K., Shao, Y., Townshend, R. F., Tsai, Y.-H., DeLong, C. J., Lopez, S. A., Gayen, S., Freddo, A. M., Chue, D. J., Thomas, D. J. et al. (2015). Lumen formation is an intrinsic property of isolated human pluripotent stem cells. *Stem Cell Reports* **5**, 954-962.

Tanos, B. and Rodriguez-Boulan, E. (2008). The epithelial polarity program: machineries involved and their hijacking by cancer. *Oncogene* **27**, 6939-6957.

Terry, S., Nie, M., Matter, K. and Balda, M. S. (2010). Rho signaling and tight junction functions. *Physiology (Bethesda)* **25**, 16-26.

Théard, D., Labarrade, F., Partisani, M., Milanini, J., Sakagami, H., Fon, E. A., Wood, S. A., Franco, M. and Luton, F. (2010). USP9x-mediated deubiquitination of EFA6 regulates de novo tight junction assembly. *EMBO J.* **29**, 1499-1509.

Torii, T., Miyamoto, Y., Nakamura, K., Maeda, M., Yamauchi, J. and Tanoue, A. (2012). Arf6 guanine-nucleotide exchange factor, cytohesin-2, interacts with actinin-1 to regulate neurite extension. *Cell. Signal.* **24**, 1872-1882.

Tushir, J. S. and D'Souza-Schorey, C. (2007). ARF6-dependent activation of ERK and Rac1 modulates epithelial tubule development. *EMBO J.* **26**, 1806-1819.

Tushir, J. S., Clancy, J., Warren, A., Wrobel, C., Brugge, J. S. and D'Souza-Schorey, C. (2010). Unregulated ARF6 activation in epithelial cysts generates hyperactive signaling endosomes and disrupts morphogenesis. *Mol. Biol. Cell* **21**, 2355-2366.

Wang, C.-C., Jamal, L. and Janes, K. A. (2012). Normal morphogenesis of epithelial tissues and progression of epithelial tumors. *Wiley Interdiscip. Rev. Syst. Biol. Med.* **4**, 51-78.

Weaver, V. M., Petersen, O. W., Wang, F., Larabell, C. A., Briand, P., Damsky, C. and Bissell, M. J. (1997). Reversion of the malignant phenotype of human breast cells in three-dimensional culture and in vivo by integrin blocking antibodies. *J. Cell Biol.* **137**, 231-245.

Wilson, P. D. (2001). Polycystin: new aspects of structure, function, and regulation. *J. Am. Soc. Nephrol.* **12**, 834-845.

Wyszynski, M., Lin, J., Rao, A., Nigh, E., Beggs, A. H., Craig, A. M. and Sheng, M. (1997). Competitive binding of alpha-actinin and calmodulin to the NMDA receptor. *Nature* **385**, 439-442.

Ye, N., Verma, D., Meng, F., Davidson, M. W., Suffoletto, K. and Hua, S. Z. (2014). Direct observation of alpha-actinin tension and recruitment at focal adhesions during contact growth. *Exp. Cell Res.* **327**, 57-67.

Zangari, J., Partisani, M., Bertucci, F., Milanini, J., Bidaut, G., Berruyer-Pouyet, C., Finetti, P., Long, E., Brau, F., Cabaud, O. et al. (2014). EFA6B antagonizes breast cancer. *Cancer Res.* **74**, 5493-5506.

Zhang, L., Li, L., Liu, H., Borowitz, J. L. and Isom, G. E. (2009). BNIP3 mediates cell death by different pathways following localization to endoplasmic reticulum and mitochondrion. *FASEB J.* **23**, 3405-3414.

Ziane, R., Huang, H., Moghadaszadeh, B., Beggs, A. H., Levesque, G. and Chahine, M. (2010). Cell membrane expression of cardiac sodium channel Na(v)1.5 is modulated by alpha-actinin-2 interaction. *Biochemistry* **49**, 166-178.

Supplementary figures

Figure S1

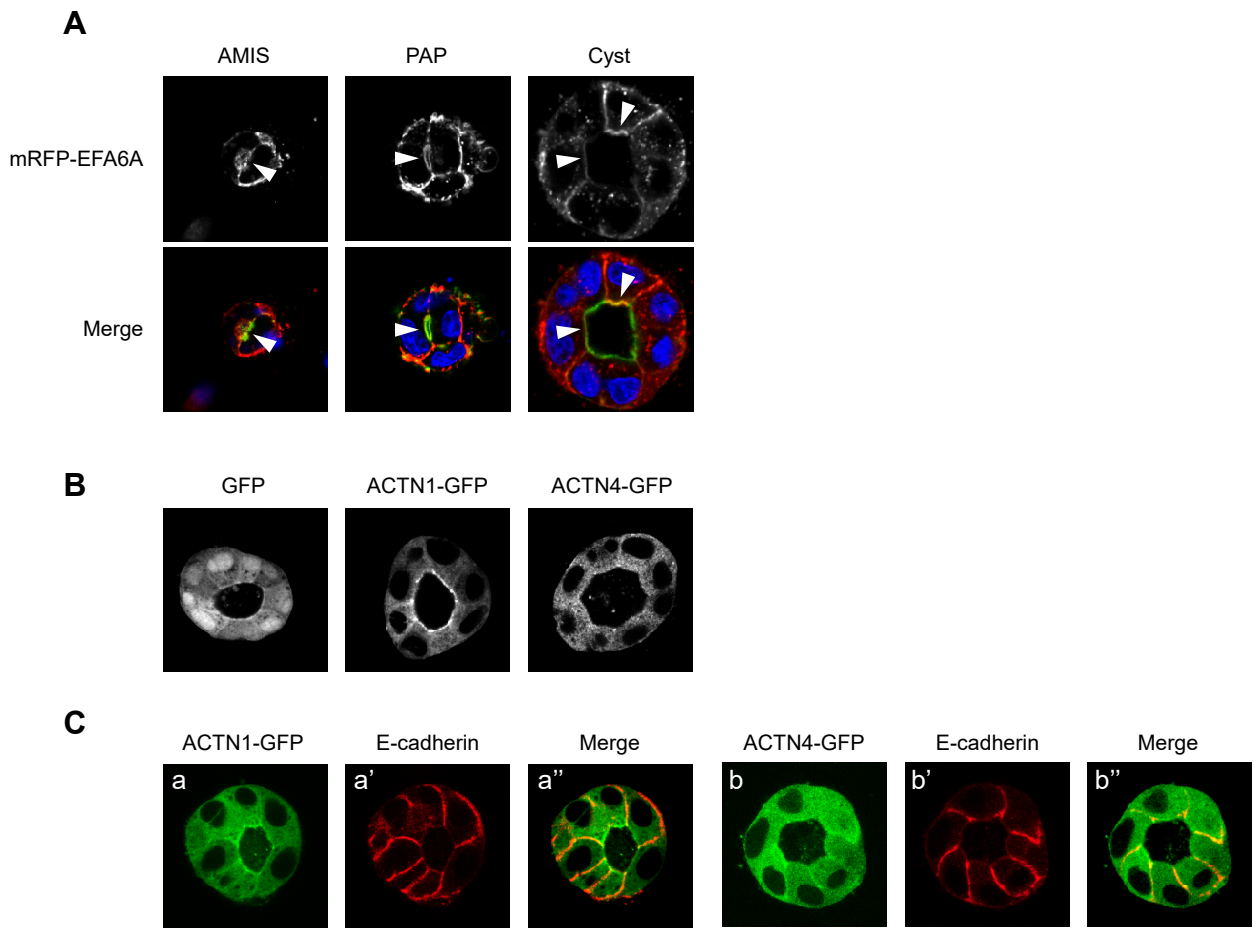

Figure S1. **Subcellular localization of mRFP-EFA6A, ACTN1-GFP and ACTN4-GFP**. **A**) MDCK cells expressing mRFP-EFA6A were grown in Matrigel and processed for immunofluorescence to label F-actin and the nuclei. The top panels show the mRFP-EFA6A staining alone and the bottom panels the corresponding merged images with mRFP-EFA6A colored in red, F-actin in green and the nuclei in blue. Scale bars 10μm. **B**) MDCK cells expressing GFP, ACTN1-GFP and ACTN4-GFP were grown in Matrigel and processed for immunofluorescence. **C**) MDCK cells expressing ACTN1-GFP (green; a-a'') or ACTN4-GFP (green; b-b'') were processed for immunofluorescence to label the endogenous E-cadherin (red). Scale bars 10μm.

Figure S2

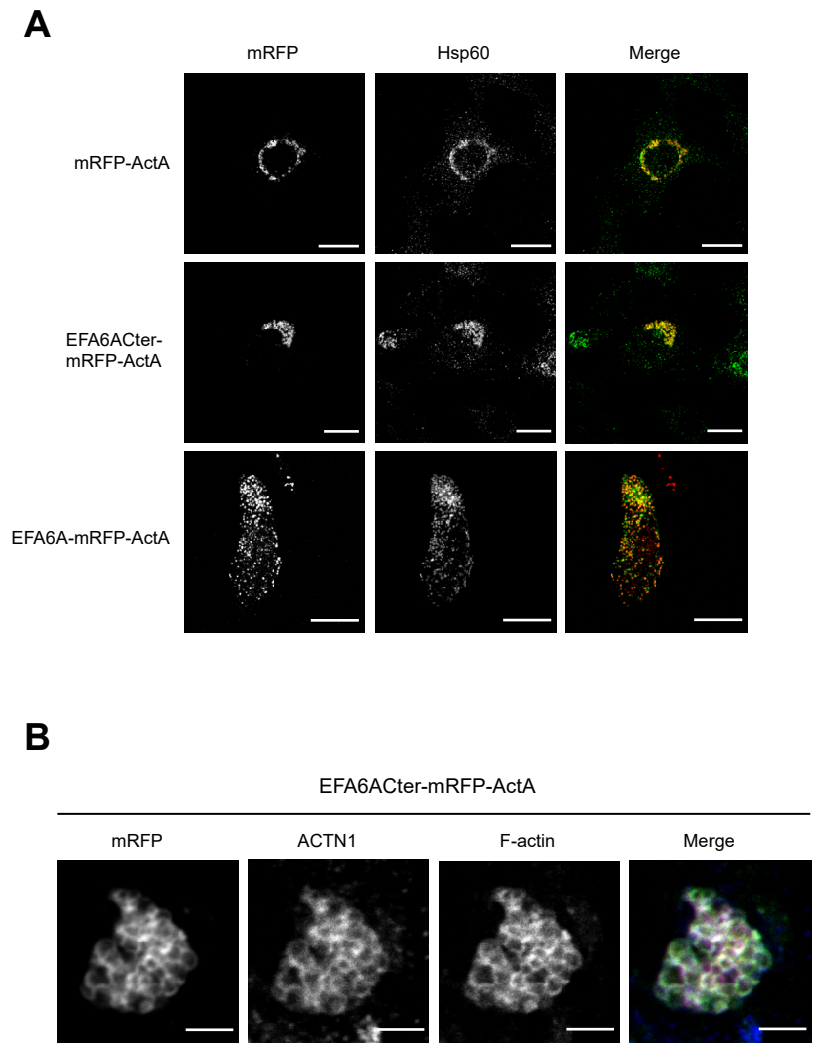

Figure S2. **A**) **The mRFP-ActA constructs localized to mitochondria**. BHK cells expressing mRFP-ActA, EFA6ACter-mRFP-ActA and the full-length EFA6A-mRFP-ActA were processed for immunofluorescence to label the endogenous mitochondrial protein Hsp60. In merge images, mRFP is colored red and Hsp60 is colored green; thus, yellow pixels indicate co-localization demonstrating that the fusion proteins are localized to the mitochondria. **B**) **Co-localization of EFA6ACter-mRFP-ActA with the endogenous ACTN1 and F-actin**. Magnified image of BHK cells expressing EFA6ACter-mRFP-ActA stained for the endogenous ACTN1 and F-actin. In the merge image, mRFP is colored red, ACTN1 is colored blue and F-actin is colored green. Overlap of expression appears white in the merge color image and indicates triple co-localization. Scale bars 10μm.

Figure S3

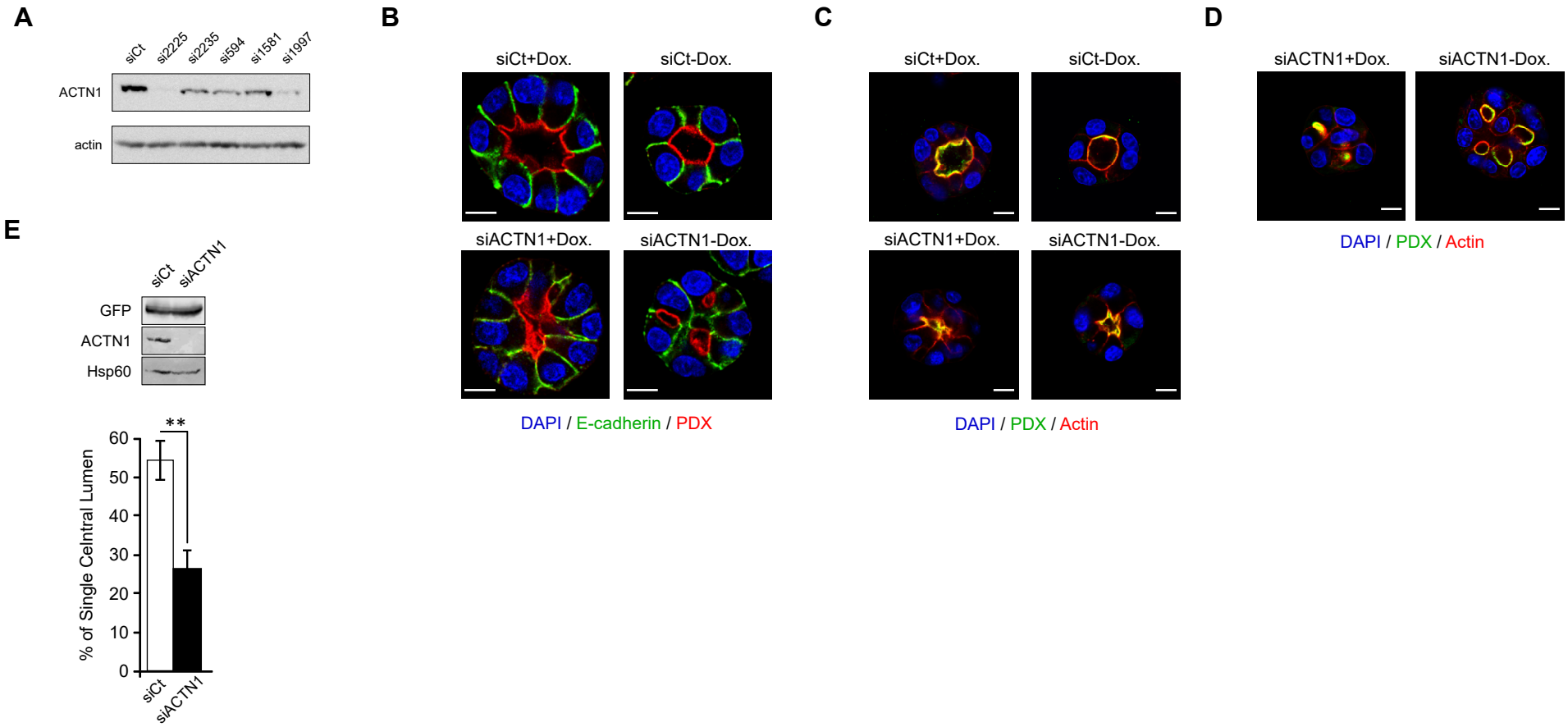

Figure S3. **A**) **siRNA-mediated ACTN1 depletion**. MDCK cells were transfected with siRNA control or siRNAs directed against ACTN1. 48 hr post-transfection the cells were solubilized in SDS lysis buffer and the expression of ACTN1 analyzed by immunoblot. Actin served as a loading control. **B**) **ACTN1 depletion does not affect the apico-basal polarity**. Inducible vsvg-EFA6A MDCK expressing cells were transfected with siRNA control or directed against ACTN1 and grown in the presence or absence of doxycycline. At day four, the cells were processed for immunofluorescence and labeled for the nuclei (blue), the AJ marker E-cadherin (green) and the apical marker PDX (red). Scale bars 10μm. **C,D**) Uncropped images shown in Fig. 3B and Fig. 3E. **E**) MDCK cells expressing GFP were transfected with siRNA control or directed against ACTN1. Top panel: the cells were solubilized in SDS lysis buffer and the expression of the indicated proteins analyzed by immunoblot. Hsp60 served as a loading control. Bottom panel: quantification of the percentage of aggregates with a SCL. Statistical significance was calculated using the Student's t-test. $n=3$, $p<0.01$.

Figure S4

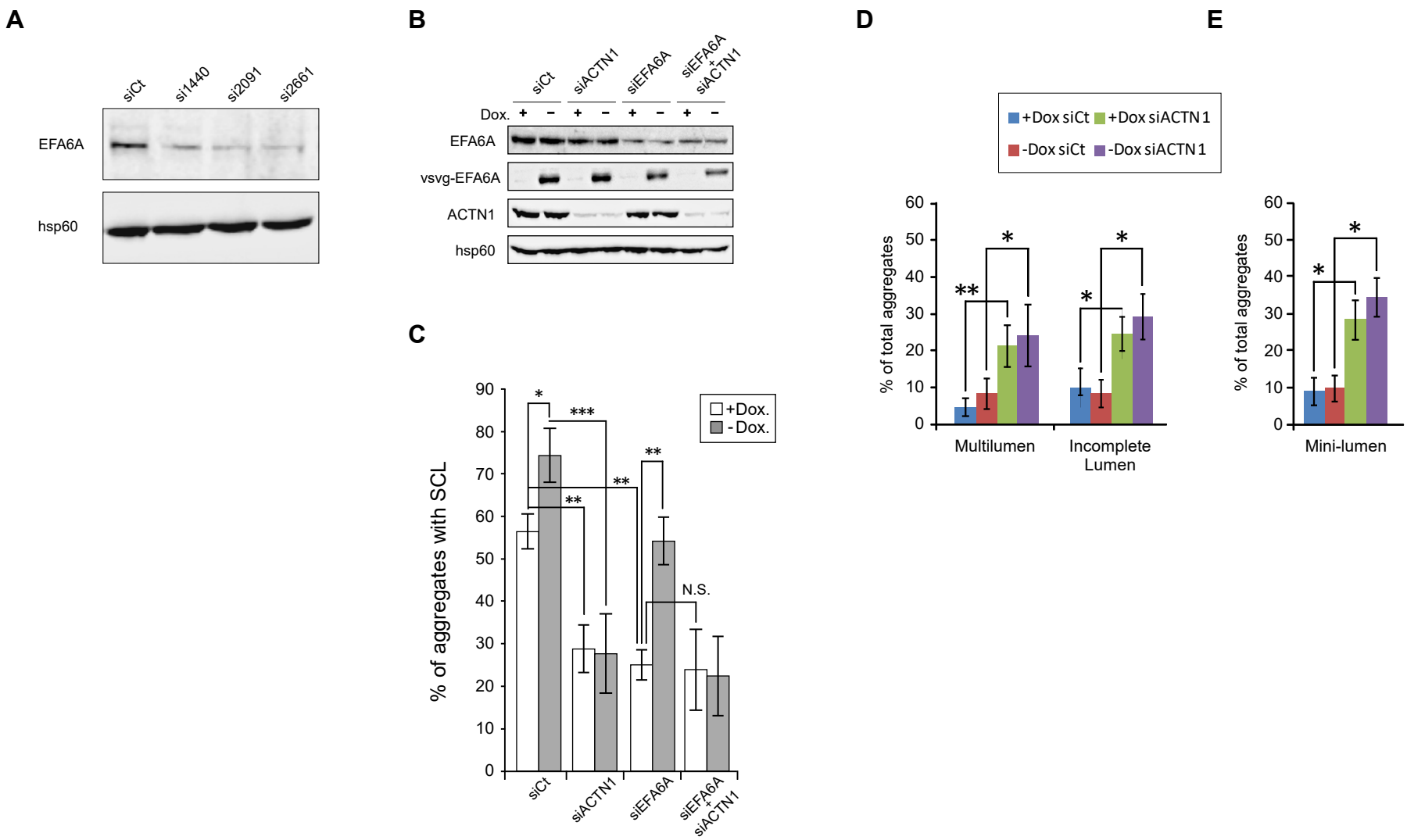

Figure S4. **siRNA-mediated EFA6A depletion.** MDCK cells were transfected with siRNA control or siRNAs directed against EFA6A. 48 hr post-transfection the cells were solubilized in SDS lysis buffer and the expression of EFA6A analyzed by immunoblot. Hsp60 served as a loading control. **B-E**) Experiments presented in Fig. 3A,B,D,E and Fig. 4A,B were repeated with alternate siRNAs directed against EFA6A (#1440) or ACTN1 (#594). *n=3, p*-values of the main results discussed in the text are indicated on the graphs.

Figure S5

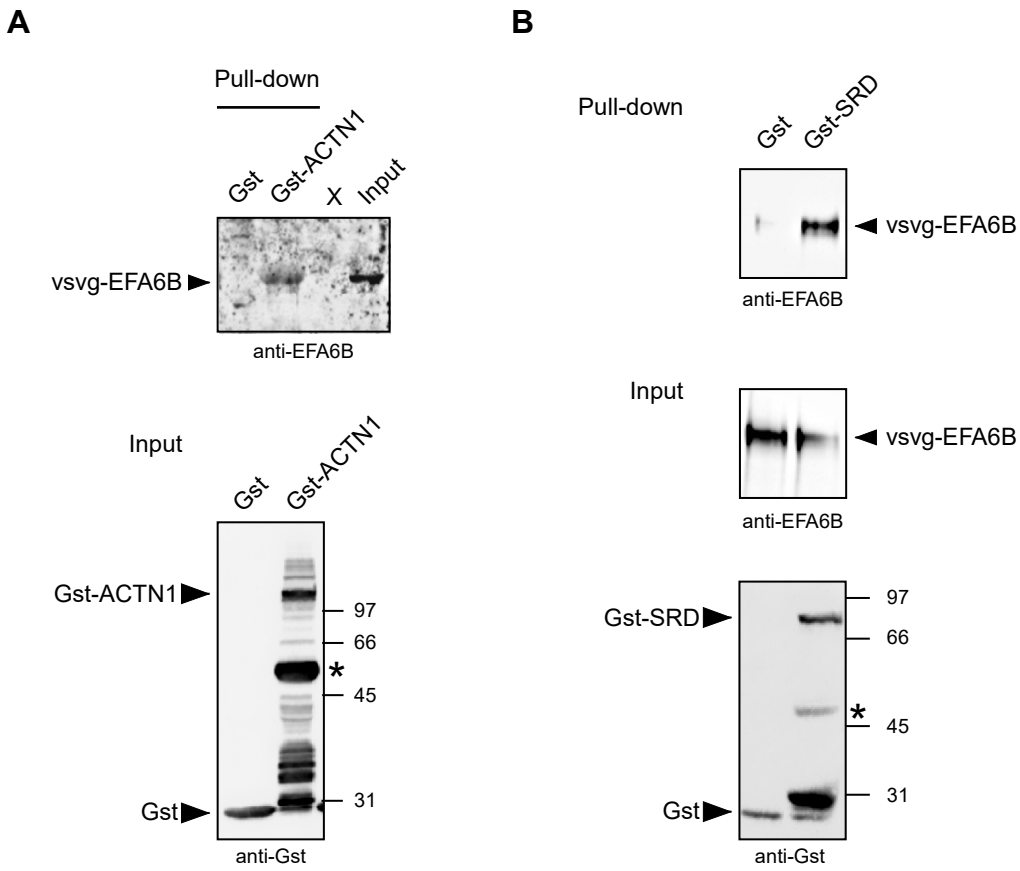

Figure S5. **EFA6B binds to ACTN1 SRD**. Lysate of MCF-10 cells expressing vsvg-EFA6B was reacted with Gst-ACTN1 (**A**) and Gst-SRD (**B**) or control Gst (**A,B**) prebound to glutathione Sepharose 4B beads. The input, whole lysate and bound proteins were analyzed by immunoblotting with the indicated antibodies. * Main purification contaminant.

Table S1. Antibodies used in this study.

Antigen	Antibody source and reference	Application	Dilution or concentration
EFA6B	Sigma-Aldrich, HPA034722	Immunoblotting	1/250
Occludin	Invitrogen, 71-1500	Immunofluorescence	1/100
pMLC	Cell Signaling Technology, 3674	Immunofluorescence	1/50
p85	Millipore, ABS234	Immunoblotting	1/500
Hsp60	Abcam, Ab46798	Immunoblotting	1/10,000
GST	GE Healthcare, 27-4577-01	Immunoblotting	1/2,000
PDX	Dr. GK Ojakian, 3B8 ascite	Immunofluorescence	1/50
VSV-G	Roche Diagnostics, P5D4	Immunoblotting	1/200
Actin	Sigma-Aldrich, AC-40	Immunoblotting	1/1,000
E-cadherin	Invitrogen, 36	Immunofluorescence	1/200
Paxillin	BD Biosciences, 610052	Immunofluorescence	1/5,000
6xHis	Sigma-Aldrich, HIS1	Immunoblotting	1/3,000
GFP	Roche Diagnostics, 7.1	Immunoblotting	1/5,000
Myc	Roche Diagnostics, 3F10	Immunofluorescence	1/100
ACTN1	Sigma-Aldrich, BM75.2	Immunoblotting	1/200
ACTN1	Santa Cruz Biotechnology, H-2	Immunofluorescence	1/100
EFA6A	Dr. H. Sakagami, immunopurified	Immunoblotting	10μg/ml